Departments of Oral and Maxillofacial Surgery
Helsinki University Central Hospital
Institutes of Dentistry and Clinical Medicine, Helsinki University
Institute of Biomedicine/ Anatomy, Helsinki University

Reconstruction of Orbital Wall Fracture
An experimental and clinical study

Risto Kontio

Academic dissertation

To be presented, with the permission of the Medical Faculty of the University of Helsinki, for public examination in the Auditorium Faltin of the Helsinki University Central Hospital, Kasarmikatu 11–13 on 23th September 2005 at 12 noon.

Helsinki 2005

Supervised by:

Professor Christian Lindqvist, MD, DDS, PhD
Department of Oral and Maxillofacial Surgery,
Helsinki University Hospital, Helsinki, Finland

Professor Yrjö T. Konttinen, MD, PhD
Department of Medicine,
Helsinki University Hospital, Helsinki, Finland

Professor Ismo Virtanen, MD, PhD
Institute of Biomedicine/Anatomy
Helsinki University, Helsinki, Finland

Reviewed by:

Docent Matti Lamberg, MD, DDS, PhD
Oral and Maxillofacial Department/ Department of Otorhinolaryngology
Kuopio University Hospital, Kuopio Finland

Professor Kyösti Oikarinen, DDS, PhD
Department of Oral and Maxillofacial Surgery,
Oulu University Hospital, Oulu, Finland

Opponent

Docent Kalle Aitasalo, MD, DDS, PhD
Department of Otorhinolaryngology - Head and Neck Surgery
Turku University Hospital, Turku, Finland

Risto Kontio
ISBN 952-91-9213-4 (nid.)
ISBN 952-10-2661-8 (PDF)
http://ethesis.helsinki.fi
Yliopistopaino
Helsinki 2005

to my family, Ulla, Ilari, Riikka, Sirke and Karri

CONTENTS

LIST OF ORIGINAL PUBLICATIONS:

The present study is based on the following publications.

I Kontio R, Salo A, Suuronen R, Lindqvist C, Meurman JH, Virtanen I. Fibrous wound repair associated with biodegradable poly-L/D-lactide copolymer implants: study of the expression of tenascin and cellular fibronectin. J Mater Sci Mater Med 9: 603-609. 1998.

II Kontio R, Suuronen R, Salonen O, Paukku P, Konttinen YT, Lindqvist C. Effectiveness of operative treatment of internal orbital wall fracture with polydioxanone implant. Int J Oral Maxillofac Surg 30: 278-285. 2001.

III Kontio R, Suuronen R, Konttinen YT, Hallikainen D, Lindqvist C, Kommonen B, Kellomäki M, Kylmä T, Virtanen I, Laine P. Orbital floor reconstruction with poly-L/D-lactide implants: clinical, radiological and immunohistochemical study in sheep. Int J Oral Maxillofac Surg 33: 361-368. 2004.

IV Kontio RK, Laine P, Salo A, Lindqvist C, Suuronen R. Reconstruction of internal orbital wall fracture with iliac crest free bone graft; clinical, CT and MRI follow up study. Plast Reconstr Surg. Accepted for publication.

V Kontio R, Al-Sukhun J, Lindqvist C. Orbital Stress Analysis. Part I: Simulation of orbital deformation following a blunt injury by finite element analysis method. Int J Oral Maxillofac Surg. Accepted for publication.

VI Kontio R, Ruuttila P, Lindroos L, Suuronen R, Salo A, Lindqvist C, Virtanen I, Konttinen YT. Biodegradable polydioxanone and poly(L/D)lactide implants: an experimental study on peri-implant tissue response. Int J Oral Maxillofac Surg Accepted for publication.

The above articles will be referred to in the text by their Roman numerals.

ABBREVIATIONS

ABC	Avidin-biotin-peroxidase complex
APAAP	Alkaline phosphatase – anti-alkaline phosphatase
CT	Computerized tomography
Da	Dalton (g/mol)
DSC	Differential scanning calorimetry
FEM	Finite element modelling
HA	Hydroxyapatite
M_n	Number-average molecular weight (g/mol)
M_W	Weight-average molecular weight (g/mol)
M_v	Viscosity average molecular weight (g/mol)
MRI	Magnetic resonance imaging
N	Newton (kgm/s^2)
Pa	Pascal (N/m^2)
PDS	Polydioxanone
PGA	Polylactide acid or polyglycolide
PLA	Polylactide acid or polylactide
PLLA	Poly-L-lactide
PLDLA	Poly-L/D-lactide
PLDLA 96/4	Poly-L/D-lactide 96/4
PLDLA 85/15	Poly-L/D-lactide 85/15
PLDLA 96/70	Poly-L/D-lactide 96/4 mesh sheet with poly-L/DL-lactide 70/30 frame
RT	Room temperature
Sil	Silicone
s.c.	Subcutaneous
SR	Self-reinforced
T_g	Glass transition temperature (°C)
T_m	Melting temperature (°C)

1. INTRODUCTION

Trauma to the orbit can result in considerable facial deformity and at the same time affect both vision and the nervous system of the face. Orbital bone fracture is in most cases open defect fracture, and this distinguishes it from other facial bone fractures. Rehabilitation of the patient requires an understanding both of the factors that cause changes in the form and function of the orbit and intra-orbital and intra-ocular tissues, and of the methods and materials available for their repair. There is general consent that the ideal material for repairing the orbital floor should be rigid enough to the support orbital contents. It should restore the original orbital form and volume, be easy to size and shape, inexpensive, readily available and most importantly, biocompatible. In short, it should be safe and user-friendly so that even inexperienced surgeons can handle it.

Until recently the treatment of choice for repairing orbital floor fractures has been autogenous bone grafting. While these grafts provide a "gold standard" for reconstructions, they are complicated in routine clinical use.

Alloplastic materials have been gaining popularity for reconstruction of the internal orbit because of their ease of use and the fact that they involve no donor-site morbidity. However, alloplastic materials have been used with caution, because some of them can provoke unpredictable foreign body reactions. As material science advances, these materials are acquiring more and more of the properties mentioned above. It is the responsibility of the surgeon to recognise the diversity of the materials available and to apply them selectively in clinical use.

It was this backround which led us to investigate the current methods and materials available for the repair of orbital fractures and to try to clarify the entire situation.

2. REVIEW OF THE LITERATURE

2.1 Anatomy of orbit, nature and clinical findings of fractures

2.1.1. Anatomy

The bony orbit has been described as a hollow pyramid made up of seven bones: maxilla, zygoma, sphenoid, ethmoidal bone, frontal bone, lacrimal bone, and palatine bone (Figure 1). It is divided into three parts from anterior to posterior. The anterior orbit is the frame and the area immediately posterior to it. The middle third of the orbit is composed of thin bone, which is anatomically very weak. The posterior third of the orbit is constructed of thick bone and incorporates the superior and inferior orbital fissures and the optic foramen.

The supraorbital section of the frame is composed of the strong inferior margin of the frontal bone. Laterally and inferiorly, the orbital rim consists of a portion of zygomatic bone. The nasoethmoidal region represents the medial rim of the orbit and extends from the junction of the maxilla with the zygoma to the frontomaxillary suture. The anterior limb of the medial canthal ligament inserts on the anterior lacrimal crest.

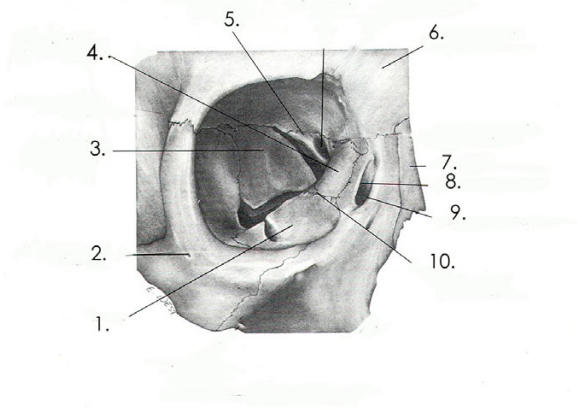

Figure 1. The right orbit viewed from the front. The orbit is surrounded by seven cranial bones (in bold): 1.= **Maxilla**, 2.= **Zygomatic bone**, 3.= Orbital aspect of greater wing of **Sphenoid**, 4.= Orbital process of **Ethmoid bone**, 5.= Lesser wing of Sphenoid, 6.= Maxillary process of **Frontal bone**, 7.= Nasal bone, 8.= Posterior **Lacrimal bone**, 9.= Anterior Lacrimal crest, 10.= Orbital process of **Palatine bone.**

The middle third includes four walls (lateral, inferior, medial, and superior). The orbital floor (inferior wall) represents a large area of anatomic weakness. The floor has an average thickness of 0.27 mm and is weakened further by the groove for the infraorbital nerve (Jones and Evans 1967). The orbital roof is a thin extension of the supraorbital rim and is composed of the greater and lesser wings of the sphenoids. The medial wall is formed largely by the thin orbital plate of the ethmoid bone. The lateral wall consists of the orbital process of the zygomatic bone and the greater wing of the sphenoid. The floor inclines superiorly at a 30 degree angle from anterior to posterior. From lateral to medial, the floor inclines at 45 degrees to merge with the thin bone of the ethmoidal

area. The complex relation creates a convex inferior and medial middle third with a concave posterior third immediately behind these.

2.1.2. Mechanism of orbital wall fracture

The anterior and middle thirds of the orbit are involved in fracture displacement, in effect acting as a shock absorber and protecting the posterior third of the orbit from severe displacement. Pfeiffer (1943) stated that from the nature of the blowout fracture it is evident that the force the eyeball is transmitted to the walls of the orbit, resulting in fractures of the thin structures (Figure 2). As a distinct entity, differing from the zygomaticomaxillary complex fracture, the term orbital "blowout fracture" was introduced by Converse and Smith (1957) and refers to a fracture of the orbital floor without an associated fracture of the orbital rim.

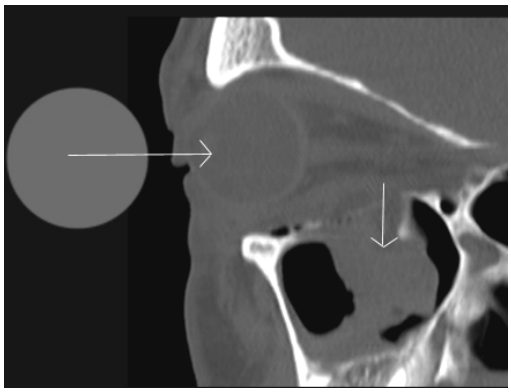

Figure 2. View in the sagittal plane of an orbit. Only the orbital walls are fractured in a pure orbital blowout fracture. This may be caused by a blunt force directed at the bony orbital rim or at intraorbital soft tissue, leading to an open defect fracture.

Smith and Regan (1957) agreed with Pfeiffer (1943) stating that a blowout fracture is caused by an impact to the orbital soft tissue, producing a momentary increase in intraorbital pressure. This is supported by other investigations (Converse *et al.* 1967, Rhee *et al.* 2002). This mechanism of blowout fracture (an increase in hydraulic pressure) has been questioned by a number of authors. According to these, when struck by a trauma force, the inferior orbital rim is sufficiently resilient to transmit the force to the orbital floor, and this may produce distant stress fractures of the orbital walls, while the rim rebounds without fracturing (Fujino and Makino 1980, Burm *at al.* 1999). Fujino (1974), in a series of experiments, on a dried human skull without orbital contents, demonstrated that a brass striker weighing 420 g with a flat silicone plate, when dropped onto the infraorbital margin from a height of 15 cm, produced a linear fracture of the orbital floor. When the weight was dropped from a height of 20 cm, a punched-out fracture in the convex portion of the orbital floor was produced. Both of these fractures occurred without fracture of the orbital rim. This is known as the bone transmission (buckling) theory. It seems that both mechanisms produce orbital floor fractures but that the orbital floor fracture may occur with lower forces by the hydraulic than by the transmission mechanism (Waterhouse *et al.* 1999, Ahmad *et al.* 2000, Ahmad *et al.* 2003).

Because of the complex structure of the orbital walls, the fracture patterns vary considerably in their location as well as in their degree of severity. The most common site of a blowout fracture is the orbital floor (Tong *et al.* 2001). The floor, the roof and the medial and lateral walls are sometimes all involved in high-energy fractures.

2.1.3. Clinical findings of orbital fractures

The clinical findings vary but may include periorbital oedema as well as enophthalmos and diplopia (Greenwald *et al.* 1974, Catone *et al.* 1988, Tong *et al.* 2001).

Enophthalmos is the result of a number of causative factors. It may occur when the periorbita is ruptured and the orbital fat escapes into the maxillary sinus (Putterman 1991) or it may be related to the traumatic atrophy of fat resulting from haematoma and a low grade inflammatory process (Putterman 1991).

On the other hand, enophthalmos may also result when the different intraorbital structures are entrapped in the fracture site, or it may be due to enlargement of the orbit resulting from the fracture and the outward displacement of the orbital walls (Pfeiffer 1943, Manson *et al.* 1986, Jin *et al.* 2000). In their retrospective study, Gilbard and

coworkers (1985) reported that enophthalmos occurred in an estimated 22% of patients with orbital wall fractures.

Binocular diplopia is one of the common symptoms of trauma involving the orbit. It is a result of deviation of the visual axes. The deviation can be caused by several factors. Entrapment of the soft tissue structures in the fracture area can interfere with muscle function (Hammerschlag *et al.* 1982). Connective tissue derangement inside the orbit can induce impaired globe mobility (Koorneef and Zonneveld 1987). Displacement of orbital walls resulting in alteration of the origin of the extraocular muscles may also modify the visual axes. Tessier (1986) suggests that diplopia is caused by nerve injury leading to oculomotor imbalance. Any damage to the cranial nerves III, IV and VI may result in binocular diplopia.

Infraorbital nerve injury is a common consequence of internal orbital wall fracture. It has been reported that 25% to 75% of patients experience some degree of infraorbital sensory disturbance after internal orbital wall fracture (Bartkowski and Krzystkowa 1982, Tong et al. 2001).

2.2. Finite element model (FEM)

The morphology of a bone is influenced by its mechanical environment and loading history (Hylander 1977, Lanyon 1987, Al-Sukhun 2003). This also applies to the orbit, and it has been suggested that the adaptive response to the functional matrix of the primate orbit is reflected in its morphology (Ravosa *et al.* 2000). Although treatment of orbital fractures has a moderate success rate, the long-term clinical significance of orbital deformation through implant treatment is still unknown. The possibility that orbital deformation and the resulting stresses may be a source of implant failure cannot be excluded. While intra-orbital techniques i.e. strain gauges provide a "gold standard" for measurements of stresses / forces, they are complex and unsuitable for clinical use. This problem, however, may in part be overcome by numerical modelling techniques, such as finite element analysis (FEA).

Why use FEA?

Insights into orbital deformation / loading have been gained from measurements of regional surface strain in living macaques (Ravosa *et al.* 2000). The extent to which these observations can be extrapolated to human beings is uncertain because of the conspicuous differences in the morphology and function between the species.

Currently, the direct measurement of bone strain in living human subjects using electrical strain gauges is impractical. Photoelastic measurements have also been performed using physical models of other bony structures such as the mandible (Ralph and Caputo 1975, Mongini *et al.* 1979, Standlee *et al.* 1981) but this technique is of limited quantitative value. As in the majority of experimental stress methods, its main disadvantage is that it is not appropriate for analysing strain under *in vivo* conditions. However, the method is non-destructive and enables the investigator to visualise the distribution of surface strains.

The most common approach has been to use mathematical modelling, where it is a much easier task to specify the locations and orientations of putative muscle tension vectors in three-dimensional space. While a few mathematical models have been reported to investigate bony structures such as the mandible and femur, no attempts have been made to build a mathematical model to study the deformation of the orbit. In these models, it has been assumed that the bone is a rigid structure, and as such behaves according to static equilibrium theory (Gysi 1921, Robinson 1946, Hylander 1975). Mathematical models necessarily assume structural rigidity and concentricity in the sagittal view, factors which complicate the analysis and limit their usefulness. Such restrictions encourage the development of models which are more representative of non-rigid, inhomogeneous structures, and which allow the simulation of wide areas of muscle attachment (Korioth and Versluis 1997, Al-Sukhun 2003). As an alternative, indirect mathematical approach, the finite element modelling technique offers the advantage of being able to model structures with intricate shapes and indirectly quantify their complex mechanical behaviour at any theoretical point.

2.3. Implant materials for orbital reconstruction

There is general consent that the ideal material for orbital floor repair should be strong enough to support the orbital contents, inexpensive, readily available, easy to contour, resorbable and most importantly biocompatible.

One of the factors that has had a direct impact on the evolution of surgical management of internal orbital fractures is the availability of numerous biomaterials for reconstructing the bony contours and restoration of the proper orbital volume. The reconstruction materials used for internal orbital fracture treatment are listed in Table 1. The main characteristics of the implant materials are listed in Tables 2. A and B.

Table 1.
Basically five different implant materials are available for orbital wall reconstruction.

Tissue grafts

Autogenous grafts	**Allogeneic grafts**	**Xenografts**
Same individual	*Same species but separate genotype (=allograft, homograft)*	*Another species*
-Bone	-Bone	-Biocoral
-Cartilage	-Cartilage	-Bone
-Dermis	-Dermis	-Dermis
-Dura mater	-Dura mater	
-Fascia	-Fascia	

Synthetic alloplastic materials

Nonresorbable	**Resorbable**
Nonmetal:	
-Bioactive glass	-Polydioxanone
-Hydroxyapatite	-Polyglycolides
-Polyethylene	-Polylactides
-Silicone	
-Teflon	
Metal:	
-Titanium	
-Vitallium	

Table 2. A.
Autogenous -, allogeneic - and xenograft materials for orbital wall reconstruction. Advantages and disadvantages of implant materials are illustrated. FF=Very favourable F=Favourable, U=Unfavourable, UU=Very unfavourable.

	Autogenous grafts		**Allogeneic grafts**			**Xenografts**	
	Bone	**Cartilage**	**Bone**	**Dura**	**Fascia/ cartilage**	**Bone**	**Dermis**
Resistance to infection, long term	FF	FF	F	F	F	F	U
Facilitates bone growth	FF	–	F	F	F	F	U
No foreign body reaction	FF	FF	F	F	F	UU	UU
Adequate mechanical properties	FF	U	FF	F	U	FF	UU
No second operative site	UU	UU	FF	FF	FF	FF	FF
No donor site morbidity	U	U	FF	FF	FF	FF	FF
Easy to harvest	F	F	FF	FF	FF	FF	FF
Easy to mold	U	F	U	F	F	U	F
Adequate in quantity	FF	F	FF	FF	FF	FF	FF
Low resorption	U	F	UU	F	F	UU	F
No risk of transmission of infectious agent	FF	FF	U	U	U	U	U

Table 2. B.
Alloplastic implant materials for orbital wall reconstruction. Advantages and disadvantages of implant materials are illustrated. FF=Very favourable F=Favourable, U=Unfavourable, UU=Very unfavourable.

	Alloplastic, nonresorbable material					**Alloplastic, resorbable material**				
	Tit	**Sil**	**Teflon**	**HA**	**BAG**	**PDS**	**PLLA**	**PLDLA**	**PGA**	**PLA/ PGA**
Resistance to infection	F	U	U	U	F	U	U	U	U	U
Facilitates bone growth	U	U	U	F	F	U	F	F	F	F
No foreign body reaction	F	U	U	F	F	U	U	U	U	U
Adequate mechanical properties	FF	F	F	F	FF	U	F	F	U	F
No second operative site	FF	FF	FF	FF	FF	FF	FF	FF	FF	FF
No donor site morbodity	FF	FF	FF	FF	FF	FF	FF	FF	FF	FF
Easy to harvest	FF	FF	FF	FF	FF	FF	FF	FF	FF	FF
Easy to mold	FF	FF	FF	F	U	F	F	F	F	F
Adequate in quantity	FF	FF	FF	FF	FF	FF	FF	FF	FF	FF
Low resorption	FF	FF	FF	F	FF	UU	F	F	UU	U
No risk of transmission of infectious agent	FF	FF	FF	FF	FF	FF	FF	FF	FF	FF

2.3.1. Autogenous grafts

Autogenous tissues were one of the first materials used to reconstruct the internal orbit (Converse and Smith 1957, Kaye 1966) and are still in frequent use today (Lai *et al.* 1998, Ellis and Tan 2003). They require a second operative site, which increasing patient morbidity and require a greater operative time to harvest. Some of them are limited in quantity, and are plagued by variable amounts of resorption over time (Sullivan *et al.* 1993). Unpredictable resorption and the potential for late occurring enophthalmos are the most critical arguments against autogenous materials. This particularly concerns autogenous bone grafts and, to a lesser degree, cartilage. Autogenous cartilage grafts are also too flexible to provide adequate support for orbital contents in larger defects (Antonyshyn *et al.* 1989). Ilankovan and Jackson (1992) reported that cartilage in its fresh state has a tendency to warp and is unsatisfactory for reconstruction of bony orbital walls.

2.3.1.1. Autogenous bone

Autogenous bone grafting has been the gold standard in providing a framework for repair of injured facial skeleton and orbital walls (Kaye 1966, Rubin *et al.* 1992, Marx 1994, Ellis and Tan 2003). The advantages of autogenous bone are its relatively good resistance to infection, its replacement by host bone in creeping substitution, the lack of a host response against the graft, and the lack of concern for late extrusion. Resorption and reduction of graft volume is obviously a concern for long-term success (Sullivan *et al.* 1993).

Basically there are two forms of nonvascularized autogenous bone grafts: cortical and cancellous (Bonutti *et al.* 1998). Cancellous grafts are revascularized more rapidly and more completely than cortical grafts. The creeping substitution of a cancellous graft initially involves appositional bone formation followed by a resorptive phase, but with cortical grafts it is *vice versa* (Buchardt 1983). Furthermore, cancellous grafts tend to repair completely whereas cortical grafts remain an admixture of necrotic and viable bone (Buchardt 1983). Cortical grafts are able to withstand mechanical forces earlier than cancellous ones and are useful for filling defects where early mechanical loading is required (Buchardt 1983). Cancellous bone imparts little mechanical strength. When cancellous bone is used to reconstruct large continuity defects, additional stabilization and rigid fixation such as a titanium mesh system are required (Tideman *et al.* 1998). The combination – a corticocancellous graft - usually produces the best results by

combining the attributes of both graft forms (De Koomen *et al.* 1979, Egbert *et al.* 1986).

Different sources such as calvarium, iliac crest, mandibular and maxillary bone, and ribs have been used (*Lee et al.* 1998, Mintz *et al.* 1998, Dempf *et al.* 2001, Siddique and Mathog 2002, Ellis and Tan 2003). At the present, calvarium bone seems to be the material of choice for orbital wall reconstruction (Dempf *et al.* 2001, Ellis and Tan 2003). Although there are multiple donor sites for autogenous grafts, the anterior iliac crest is the most common (St John *et al.* 2003).

Autogenous bone graft from the anterior iliac crest is a favourable reconstruction material because enough bone is always available and bone can be harvested simultaneously with the orbital exploration. However, an iliac crest bone graft is said to be bulky unless trimmed and it may resorb unpredictably. Both de Visscher and van der Wal (1988) and Bartkowski and Krzystkowa (1982) used iliac crest graft for orbital floor or medial wall reconstruction in their follow-up studies and concluded that autogenous corticocancellous bone like iliac crest is very well tolerated and is an adequate material for orbital wall reconstruction. Their results are similar to those of many other researchers (Roncevic and Malinger 1981, Sullivan *et al.* 1993, Dempf *et al.* 2001, Ellis and Tan 2003). Donor site disadvantages of autogenous iliac bone graft include nerve and blood vessel injuries, chronic pain, gait disturbances and cosmetic nuisance. In the light of the high numbers of autologous iliac crest grafts used, the donor site morbidity seems to be low (Banwart *et al.* 1995, Ahlmann *et al.* 2002).

2.3.2. Allogeneic grafts

An allogeneic graft is a living or preserved tissue of one individual transferred to another of the same species but with a different genotype. In the literature, allogeneic implants are also referred to as allografts or homografts. Isograft or isogeneic graft refers to a tissue graft transplanted from one individual to another, who is genetically identical. Allogeneic material may include allogeneic bone, cartilage, dura and fascia. These materials contain no living cells and become incorporated into host tissues by providing a structural framework for ingrowth of host tissues. They do not require a second operative site and are generally abundant in supply. Allogeneic materials have been successfully used for orbital wall reconstruction. However, the use of allogeneic grafts is decreasing because of concern over the antigenicity of the material and the potential transmission of infectious diseases (Burchardt 1983, Thadani *et al.* 1988).

2.3.3. Xenografts

A xenograft is non-vital tissue that is harvested from one species and transferred to the recipient site of another species. Both soft tissue and bone grafts are available.

Xenogeneic bone was popular in the 1960's but fell into disfavour due to reports of patients developing autoimmune diseases following bovine bone transplants (Pieron *et al.* 1968, Buchardt 1983). In theory, the transmission of infectious diseases is possible when xenografts are used, although no such reports seem to be available in the literature.

Xenografts are rarely used for the repair of internal orbital fractures. Only a few case reports are available in the literature regarding their application within the orbit. A severe inflammatory reaction with the granulomatous component has been reported after the use of porcine dermis in orbital wall reconstruction (Converse *et al.* 1967, Webster 1988, Morax *et al.* 1993, Cheung *et al.* 2004).

2.3.4. Alloplastic materials

Alloplasts have gained popularity for reconstruction of the internal orbit because of their ease of use and the fact that there is no donor-site morbidity. Other benefits of alloplasts include shorter operation times, the large variety of sizes and shapes available, and their seemingly endless supply.

2.3.4.1. Nonresorbable

Nonresorbable alloplastic materials include: titanium, silicone, polytetrafluoroethylene, polyethylene, hydroxyapatite and bioactive glass.

Titanium

Titanium plates are thin, stiff and easy to contour. They are easily stabilized, maintain their shape, and have the unique ability to compensate for volume without the potential for resorption. When titanium plates were introduced, it was generally believed that they needed no removal, since titanium is a highly biocompatible material (Breme *et al.* 1988). However, it has been shown that both titanium and aluminium are released from titanium implants into the adjacent structures and even into regional lymph nodes (Moberg *et al.* 1989, Onodera *et al.* 1993, Katou *et al.* 1996). The clinical relevance of this release is not yet known. It has been suggested that in paediatric surgery in the

areas of bony resorption and deposition, metallic fixation plates should be removed due to plate displacement and to restriction of growth (Fearon *et al.* 1995).

There are further disadvantages with titanium implants in orbital wall reconstruction. These include the risk of extrusion due to dehiscence of covering soft tissue and the risk of infection. There is also a theoretical risk of injury to the tissues of the orbital apex from any subsequent blow to the orbit. Because of the mesh structure, the orbital implant is difficult to remove (Sugar *et al.* 1992).

Titanium implants have been used to span large defects in the internal orbit to provide a platform for bone graft support. This technique proved to be reliable and bone graft positioning was more secure. The infection rate was reported to be 5% (Glassman *et al.* 1990). It was not until the report by Sargent and Fulks (1991) that metals alone were routinely used for orbital reconstruction without an intervening bone graft or alloplast between the metal and the orbital soft tissues. Many researchers have concluded that titanium mesh implants are a simple and reliable option for routine orbital floor repair (Sugar *et al.* 1992, Mackenzie *et al.* 1999, Ellis and Tan 2003).

Rubin and coworkers (1992) compared the use of custom-shaped orbital floor titanium plates or vitallium mesh with autogenous bone grafts. They reported no significant complications related to the orbital implants. Metal implants were easier to use than autogenous bone grafts.

Silicone, polytetrafluoroethylene and polyethylene

Silicon (Si) is the second most abundant element on earth, comprising around 28% of all matter. Silicones (polyorganosiloxanes) are synthetic polymers of silicon and oxygen (known as siloxane) modified with various organic groups attached to the silicon atoms. These organic molecules prevent the formation of the three-dimensional network characteristic of silica. Silicone rubber is a chemically inert material available in block and sheet forms. Polytetrafluoroethylene (Teflon®) is a long-chain halogenated carbon polymer made by the polymerization of tetrafluoroethylene gas at high temperature and pressure. Both materials evoke a mild fibroblastic or inflammatory reaction (Lossing and Hansson 1993, Cashman *et al.* 2002, Ward *et al.* 2002, Reno *et al.* 2003). Both have been used for orbital wall reconstruction even though they are neither osteogenic nor osteoconductive nor osteoinductive. Widely varying complications have arisen from the use of these alloplastic implants, such as inferior eyelid swelling, pain, ocular dystopia and maxillary sinusitis, extrusions and local

infections (Aronowitz *et al.* 1986, Dufresne *et al.* 1988, Morrison *et al.* 1995, Pauzie *et al.* 1997, Rubin and Yaremchuk 1997).

Solid polyethylene, the structural component of porous polyethylene, is a highly inert material. It is synthesized by the polymerization of ethylene. A porous polyethylene implant is a biocompatible material composed of high-density polyethylene microspheres sintered to create a framework of interconnected pores. Its porous character allows for rapid fibrovascular and soft tissue ingrowth and eventual incorporation of bone.

High-density porous polyethylene (HDPP) has been used extensively for craniofacial reconstructive procedures. HDPP implants have been used successfully for correction of mild to moderate posttraumatic enophthalmos (Karesh and Horswell 1996). In a series of 140 patients, there was just one instance of implant infection requiring removal, and no implant migration or exposure (Romano *et al.* 1993). Other investigators too, have concluded that porous polyethylene sheets offer advantages when used for orbital reconstruction. They seem to permit predictable, stable results with few complications (Rubin *et al.* 1994).

Hydroxyapatite

Hydroxyapatite (HA) can be manufactured from natural reef-building coral skeleton by a hydrothermal exchange reaction, where the trabecular, bone imitating structure of the coral remains unchanged but the calcium carbonate (CC) skeleton is converted to calcium phosphate, the main inorganic salt of bone (Roy and Linnehan 1974). HA has been used for both primary and secondary reconstruction of the orbital walls. Both HA block scaffolding and computer-aided machined HA ceramic implants have proved to be useful alternatives to metallic floor implants and autologous bone grafts in the reconstruction of large traumatic orbital floor defects (Hes and de Man 1990, Ono *et al.* 1994, Lemke and Kikkawa 1999).

Bioactive glass

Bioactive glasses (BAGs) are silicates containing sodium, calcium, and phosphate as their main network modifier components. The glassy network of BAG binds to bone by a surface layer of hydroxyapatite that forms through chemical reaction with the glass. This chemical bonding of BAG and bone has been demonstrated by several investigators (Hench and Paschall 1973). It has proved to be biocompatible and

nontoxic (Wilson *et al.* 1981, Gross and Strunz 1985, Aitasalo *et al.* 2001). Bioactive glass is osteoconductive in humans (Schepers *et al.* 1993, Furusawa and Mizunuma 1997, Tadjoedin *et al.* 2000). Studies have demonstrated that bioactive glass particles of narrow size range (300-355 μm [Biogran®]) have the capacity to stimulate bone tissue formation without contact with pre-existing bone (Huygh *et al.* 2002).

Good results have been achieved with this material in frontal sinus surgery (Peltola *et al.* 1998). Only a few studies are available on the use of bioactive glass in orbital wall reconstruction. In a prospective study Kinnunen *et al.* (2000) compared the use of bioactive glass with conventional autogenous grafts (cartilage with or without lyophilized dura) for the repair of orbital floor defects after trauma. They concluded that bioactive glass was well tolerated and showed adequate maintenance of orbital and maxillary sinus volume without any evidence of resorption in either group.

2.3.4.2. Resorbable

Biodegradable polymers (Figure 3) have been used for biomedical applications for many years. Polyglycolide, polylactide, and polydioxanone all degrade *in vitro* and *in vivo* by hydrolysis. Enzymatic activity enhances the hydrolysis, degradation being more rapid in tissue environment than in vitro (Williams 1982).

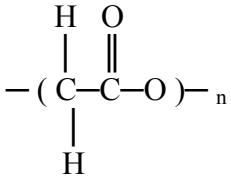

Polyglycolide

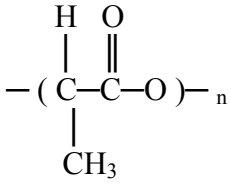

Polylactide

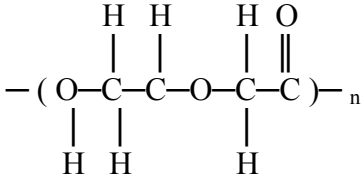

Polydioxanone

Figure 3.
PGA and PLA are synthesized by ring opening polymerization of the cyclic diesters of glycolic acid and lactic acid respectively. PDS is a high molecular weight crystalline polyester of para-dioxanone.

Polydioxanone (PDS)

PDS is a biodegradable material that loses 50% of its strength in the first postoperative month (Merten and Luhr 1994). It is a high molecular weight, colourless crystalline polyester of para-dioxanone. The glasstransition temperature of PDS is -16° C. At this temperature the material becomes brittle and rigid. Its melting point is 110^{o} C (Doddi *et al.* 1977). At room temperature PDS is rubber-like and ductile.

The degradation products of PDS are excreted mainly in the urine, but some are excreted in the feces and exhaled as CO_2 (Ray *et al.* 1981). *In vivo* experiments on rats showed a slight tissue reaction (Knoop *et al.* 1987). PDS is completely absorbed after 6 months (Hidding *et al.* 1991). PDS has been mainly used in sutures, cords, pins, and screws in experimental and clinical orthopaedic surgery (Claes *et al.* 1986, Mäkelä *et al.* 1989, Riedl and Genelin 1991, Plaga *et al.* 1992). It is usable in soft tissue, tendon, and ligament surgery because of its flexibility (Vainionpää *et al.* 1989). PDS has been reported to be well tolerated by the body and does not give rise to clinically detectable inflammatory reactions (Knoop *et al.* 1987, Mäkelä *et al.* 1989).

New bone formation has been noted when PDS has been used for orbital wall reconstruction (Cantaloube *et al.* 1989). PDS seems to be easy to cut to suitable sizes and retains its structural integrity long enough for a sufficiently rigid scar to be formed (Cantaloube *et al.* 1989, Iizuka *et al.* 1991). Because of resorption of the thick plate, overcorrection was thought to be necessary (Iizuka *et al.* 1991). Other studies corroborated earlier findings. PDS can be shaped and adjusted, is mechanically good enough for orbital reconstruction, and resorbs within one year. Overall results seem to be acceptable (Hidding *et al.* 1991, Jank *et al.* 2003).

However, some studies have shown less favourable outcomes related to PDS. Lack of osteoconductive properties was documented by Baumann and coworkers (2002). These authors concluded that large defects in the orbital floor (more than 2.5 cm^2) cannot be reconstructed with PDS sheet, which should be used only in cases without massive orbital fat herniation. Merten and Luhr (1994) and later de Roche and coworkers (2001) agreed with these results and further showed that PDS provokes adverse foreign body reactions. PDS orbital implants are not available in the United States.

Polylactide (PLA) and polyglycolide (PGA)

PLA is a pale-coloured, semicrystalline polymer with a glasstransition temperature of 57° C and a melting point of 174° C (Vert *et al.* 1981, Törmälä *et al.* 1998), (Figure 3).

PLA can exist in four forms, depending on the L – and D – configuration (Holten 1971). If the polymer consists only of the L isomer, it is called poly-L-lactide acid, PLLA, which has most commonly been used for orthopaedic implants. If it contains both isomers, it is a stereocopolymer, called poly-D/L-lactide acid, often referred to as P-L/DL-LA or PLDLA. PLDLA is more amorphous and less crystalline and thus degrades faster than pure PLLA (Kulkarni *et al.* 1971).

PLLA implants have been used for orbital floor reconstruction since 1972, when Cutright and Hunsuck (1972) published an *experimental study* on rhesus monkeys using 1.5 mm thick PLLA sheets. They reported normal healing of the fracture and normal globe movements. The PLLA sheets were resorbed by phagocytes and giant cells with villous projections. Residual PLLA was detectable after 38 weeks. No inflammatory reactions were seen. Similar findings were reported later by Rozema and coworkers (1990). In a study by Cordewener and coworkers. (1996) the long-term outcome was evaluated after the repair of orbital floor defects in *patients* with resorbable as-polymerized PLLA implants in order to determine whether these patients showed symptoms that could be indicative of the presence of a late tissue response. In the preceding years none of the patients had experienced any problems such as infection, migration, or extrusion of the implants, all of which might have indicated complications. The main drawback of PLLA implants, however, is its low degradation rate and slow resorption in clinical use (Bergsma *et al.* 1993, Tams *et al.* 1996, Suuronen *et al.* 1998).

P-L/DL-LA implants have been used in an *experimental* study in rats. There were no signs of inflammation. The histological image of P-L/DL-LA 96/4 after 55 weeks closely resembled the image observed for PLLA in rats after 143 weeks. Because of the relative loss of mechanical properties osteosynthesis made with P-L/DL-LA 96/4 may be suitable only for applications under low biomechanical load (Cordewener *et al.* 1995). Self-reinforced (SR) P-L/DL-LA plates and screws have been used *clinically* in orthognathic and trauma surgery. The short-term follow-up has been comparable to the "gold standard" of titanium plates and screws (Haers and Sailer 1998, Ylikontiola 2004). No clinical foreign-body reactions caused by SR P-L/DL-LA devices have been reported (Suuronen 1993).

PGA is a hard crystalline polymer which, when possessing fibrous properties, has a molecular weight from 20000 to 145000 (Frazza and Schmitt 1971). SR PGA implants were used to treat 20 blowout fractures (Sasserath *et al.* 1991). Two *patients*

complained of continuous infraorbital oedema, which, according to the authors, was caused by poor residual drainage. The problem was solved by regular massage of the region.

Copolymers of biodegradable polyglycolide and polylactide acids have been used for fracture treatment. *Experimental* studies have shown that this copolymer has a more rapid rate of degradation (9 to 15 months) than PLLA and therefore might be more suitable as an orbital implant material (Bahr *et al.* 1999, Wiltfang *et al.* 1999). *Clinical* studies have shown good results with Lactosorb® throughout the craniofacial skeleton (Ahn *et al.* 1997, Enislidis *et al.* 1997).

2.4. Tissue repair

2.4.1. Osteogenesis, osteoinduction, osteoconduction

Blowout fracture refers to a state where the walls of the orbit have fragmented, leading to a bone defect (Pfeiffer 1943). The aim of modern reconstruction should be to facilitate new bone formation over the defect area. New bone formation occurs via three biological mechanisms: osteogenesis, osteoinduction and osteoconduction. The implant used for blowout fracture repair should promote one or more of the above mechanisms leading to defect repair.

Osteoblasts of the transplanted bone graft and of fractured bone are responsible for new bone formation, i.e. **osteogenesis**. Osteoblasts survive for up to five days post-transplantation due to their ability to absorb nutrients from the surrounding tissues (Caplan 1994). The mineralized matrix of cortical bone is relatively impervious and nutrition by diffusion alone will predominantly affect those cells at or near the surface of the graft in contact with the host tissue. Therefore, cells of the periosteum and endosteum at the edges of cortical bone grafts survive (Motoki and Mulliken 1990). Entrapped platelets inside the graft release potent growth factors (Caplan 1994) and endothelial cells initiate capillary ingrowth. Stem cells start to differentiate into osteoblasts, which together with endosteal osteoblasts from the transplanted bone start to lay down osteoid (Marx 1994).

Osteoinduction is the formation of bone by connective tissue cells transformed into osteocompetent cells by inductive agents, usually proteins such as bone morphogenetic protein. Urist (2002) was the first to describe the osteoinduction mechanism in 1965. Since then, a wide variety of entities having different effects on bone have been discovered. They are classified as osteoinducers, osteopromoters or bioactive peptides.

Human bone morphogenetic proteins as an aid for fracture treatment have been successfully used in Finland (Govender *et al.* 2002).

Osteoconduction describes bone formation by the process of ingrowth of capillaries and osteoprogenitor cells from the recipient bed into, around and through a graft or implant which acts as a scaffold for new bone formation. Unlike osteoinduction, this process occurs in an environment already containing bone.

2.4.2. Wound healing

Wound healing involves many complicated, concurrent events and can be divided into three overlapping phases: an inflammation phase, a granulation tissue formation phase, and a matrix formation/ remodelling phase. Interactions of the individual components of extracellular matrix (ECM) with specific cell surface molecules initiate a cascade of signal transduction. These transductions lead to varied cellular responses (Raghow 1994).

During the first stage (day 1 – day 3), neutrophils and monocytes appear in the wound space and mediators are released that then set the stage for the formation of granulation tissue (Gailit and Clark 1994). The second phase (day 4 – day 6) of wound healing is characterized by granulation tissue formation. The processes of angiogenesis, re-epithelialization, and collagen synthesis occur. Important in granulation tissue formation is the development of an ECM (Gailit and Clark 1994). Remodelling is the third phase of wound healing (day 7 –). ECM is revamped and the collagen is converted from type III collagen to type 1 collagen. As remodelling proceeds, fibronectin disappears from the wound and is replaced by collagen. A gradual loss of cells and vasculature is detected during this phase (Raghow 1994). Also during this stage wound contraction occurs. A delicate balance in the biosynthetic and degradative pathways of ECM restructuring may swing this pendulum towards tissue remodelling or fibrosis.

The wound contraction phenomenon is generally attributed to myofibroblasts, which are found in granulation tissue. This may last for several weeks (Ehrlich 1988). During the wound healing process, these cells produce tenascins and cellular fibronectin, both of which provide trophic support in the connective tissue (Mackie *et al.* 1988, Whitby and Ferguson 1991).

Tenascins (Tn) and Fibronectin (Fn)

Tenascins are members of a large ECM glycoprotein family. The vertebrate tenascin family consists of at least three and possibly four member proteins, built up by the structural domains typical of the tenascins (Chiquet-Ehrismann *et al.* 1994). The functions of the tenascins are still largely unknown. Tiitta and coworkers (1992) have shown a prominent tenascin immunoreaction in inflammatory lesions. During wound healing, tenascins are present throughout the matrix of the granulation tissue, which fills full-thickness wounds, but is not detectable in the scar after wound contraction is completed (Mackie *et al.* 1988). Luomanen and Virtanen (1993) studied the distribution of extracellular matrix tenascin in normal mucosa and during healing of scalpel-incised or excised and CO2 laser-wounded rat tongue dorsal mucosa. According to their study the immunoreactivity to tenascin diminishes to almost normal 11 days after the operation. The overall tenascin staining is greatly increased in the synovial membrane-like interface tissue between implant and bone in aseptic loosened hip prosthesis compared with synovial membrane and fibrous capsule from primary total hip replacement operations (Konttinen *et al.* 1998). When the cellular and molecular compositions of fibrous capsules removed from around silicone breast implants were studied, a massive deposition of tenascin was observed adjacent to the implant surface (Dolores *et al.* 2004).

Fibronectin is of key importance in wound healing and is involved in all its phases (Luomanen and Virtanen 1991, Whitby and Ferguson 1991). Fibronectin is chemotactic for fibroblasts and macrophages (Nagelschmidt *et al.* 1987). Fibronectin plays a major role in the second phase of wound healing. The scaffolding helps fibroblasts and epithelial cells migrate over and through the extracellular matrix. This temporary basement membrane allows for the phenotypic and mitogenic changes noted in these cells during wound healing (Luomanen and Virtanen 1991). Only a few studies are available about cellular fibronectin (cFn) expression in connective tissue capsules around implanted materials. Dolores and coworkers (2004) analyzed of the cellular and molecular compositions of fibrous capsules removed from around silicone breast implants with complications in patients at various times after primary surgery and observed massive deposition of fibronectin adjacent to the implant surface.

When synovial membrane-like interface tissue after aseptic loosening of prosthetic components was compared with osteoarthritic synovial membranes, expression of fibronectin had a similar distribution pattern in both tissues (Konttinen *et al.* 2001).

2.4.3. Peri-implant connective tissue capsule

The mechanisms controlling the formation of peri-implant connective tissue capsule and the reactive and adaptive changes in it are not known. The mechanism seems to be linked to the low-grade chronic inflammation caused by the foreign body reaction (Asplund 1984, Ksander and Vistnes 1985, Burkhardt 1988, Bagambisa *et al.* 1994, Santavirta *et al.* 1998). Operative trauma, implant instability and corrosion/friction are recognized as aetiological factors in the production of the soft-tissue capsule which is often present around metal implants (Linder and Lundskog 1975, Goodman 1994, Santavirta *et al.* 1999). It has been demonstrated that the surface texture of an implant is also an important variable in determining the soft tissue response to a material and fibrous capsule formation (Taylor and Gibbons 1983, van Mullem *et al.* 1990). The peri-implant fibrous capsule contains cells including myofibroblasts (Lossing and Hansson 1993). They are unique smooth muscle-like fibroblasts that contain cytoskeletal α-actin bundles. They seem to generate contractile forces that produce wound contraction and peri-implant capsule contracture (Welch *et al.* 1990, Lossing and Hansson 1993).

3. AIMS OF THE STUDY

The materials used to repair orbital defects have been broadly categorised as autologous and alloplastic. Autologous materials are generally biodegradable, while alloplastic materials are subdivided into biodegradable and non-biodegradable materials. The main aim of the present study was to investigate the clinical properties and biocompatability of orbital reconstruction materials and to produce recommendations for selection of these materials for routine clinical use.

The specific objectives were:

1. To study the mechanical properties of PDS sheets and to assess whether they provide adequate support for orbital contents in clinical use in order to prevent posttraumatic enophthalmos and hypo-ophthalmos.

2. To study whether the mechanical properties of SR PLDLA 85/15, SR PLDLA 96/4 and SR PLDLA 96/70 composite implants are appropriate for orbital wall fracture reconstruction.

3. To study the distributions of Tn, cFn, α-actin and type I and type III collagen in the connective tissue capsule of PDS, SR PLDLA 85/15, SR PLDLA 96/4 and SR PLDLA 96/70 composite implants, and to study host response to these materials to assess their biocompatibility in possible clinical use

4. To study whether autologous iliac bone graft restores the shape and volume of a fractured orbit, provides adequate support for orbital contents and facilitates new bone growth across the orbital wall defect to restore the orbital volume and to prevent posttraumatic enophthalmos and hypo-ophthalmos.

5. To develop a three-dimensional finite element model of the human orbit and to use it to study the stresses and strains required to produce traumatic orbital fractures and deformations.

4. MATERIALS AND METHODS

Essential data, materials and follow-up times used in these experimental and clinical studies is given in Table 3.

Table 3.
Materials, follow-up times and properties of implants used in experimental and clinical studies. Roman numerals refer to the number of the original publication.

Study	**Rabbit (I)**	**Sheep (III)**
Number of animals / implants	10 / 60	18 / 18
Implant placement	Dorsal subcutis	Orbital floor
Follow-up	4, 12, 16, 36 and 48 weeks	12 , 16, 22 and 36 weeks
Material	SR poly-L/D-lactide acid stereocopolymer	SR poly-L/D-lactide acid stereocopolymer
Structure	plate (SR PLDLA 85/15)	plate (SR PLDLA 96/4)
Molar ratio	85/15	96/4, low monomeric <0,16%
Manufacturer	Institute of Biomaterials, Tampere University of Technology, Finland	Institute of Biomaterials, Tampere University of Technology, Finland
Raw material	Purac biochem	Purac biochem
Sterilization	Ethylene oxide or gamma irradiation	Gamma irradiation

Study	**Rat (VI)**	**Rat (VI)**	
Number of animals / implants	12 / 12	12 / 12	
Implant placement	Dorsal subcutis	Dorsal subcutis	
Follow-up	2, 3, 4 and 5 months	3, 4, 5 and 7 months	
Material	PDS®	SR poly-L/D-lactide acid stereocopolymer mesh sheet	SR poly-L/DL-lactide acid stereocopolymer frame
Structure	folio	Combined mesh sheet and frame, plate (SR PLDLA 96/70)	
Molar ratio		96/4	70/30
Manufacturer	Ethicon, Nordenstedt, Germany	Institute of Biomaterials, Tampere University of Technology, Finland	Institute of Biomaterials, Tampere University of Technology, Finland
Raw material		Purac Biochem b.v. Netherlands	Boehring Ingelheim, Germany
Sterilization	Gamma irradiation	Gamma irradiation	Gamma irradiation

Study	**Human (II)**	**Human (IV)**
Number of patients / implants	16 / 16	24 / 24
Implant placement	Orbital floor	Orbital floor
Follow-up	1, 2, 4, 8, 12, 36 weeks	1, 2, 4, 8, 16 and 36 weeks
Material	PDS®	Iliac crest graft
Structure	Folio	Corticocancellous free graft
Manufacturer	Ethicon, Johnson&Johnson, Brussels, Belgium	Autogenous
Sterilization	Gamma irradiation	

4.1. Experimental studies (I, III, VI)

The experimental studies included three different implant models with four types of implants using rabbit (I), sheep (III) and rat (VI) as research animals. For methodological details see the original publications. The mechanical properties of polydioxanone (PDS®) orbital wall implant and three types of poly-L/D-lactide implants were evaluated and compared. Immunohistochemistry, microscopy and electron microscopy studies were performed.

4.1.1. Animals, anaesthesia, follow-ups

Experimental study using rabbits (I)

Ten rabbits were anaesthetized with subcutaneous (s.c.) ketamine (Ketalar®, Parke-Davis, Barcelona, Spain) 25 mg/kg and medetomiden (Domitor®, Lääke-Farmos, Turku, Finland) 0.3 mg/kg. Two animals were sacrificed at each follow-up time.

Experimental study using sheep (III)

Anaesthesia for the 18 sheep used in these experiments was induced using Propofol 2 mg/kg (Rapifen, Zeneca Ltd., Cheshire, UK) and maintained with 2-2.5% halothane in oxygen using an open ventilation system following intubation. At each follow-up respectively 5, 4, 4 and 5 animals were sacrificed.

Experimental study using rats (VI)

24 adult male E.DA/KS:Fi rats were anaesthesized using a fentanyl-fluonison combination (1,5 ml/kg s.c., Janssen-Cilag, Sanderton, U; Hofmann La Roche, Basle, Switzerland). Three animals were sacrificed at each follow-up

4.1.2. Operative techniques

Experimental study using the rabbit model (I)

SR PLDLA 85/15 plates were inserted into the dorsal subcutaneous tissue. The two control rabbits were operated on in the same manner but without implantation. After the follow-up the plates and surrounding connective tissues were carefully removed. In the control animals the scar and connective tissue were removed from the operated region.

Connective tissue capsules enveloping the plates were examined using haematoxylin-eosin staining and immunohistochemistry. The mechanical properties of the implants were analyzed.

Experimental study using the sheep model (III)

Both orbital floors were exposed using an infraorbital approach. The periosteum was elevated and the floor was cut open with a burr and chisel. The defects created were 10 mm x 20 mm in size. The orbital content was repositioned and the floor was reconstructed using a PLDLA 96/4 plate. The implant was fixed to the orbital floor with two micro tacks. No reconstruction was performed in the contralateral orbital floor.

After the follow-up the orbital floors were exposed. The floors were photographed and measured. Implants were removed for further mechanical analyses together with tissue samples from the superior surface of the connective tissue capsule for immunohistochemical studies.

Experimental study using the rat model (VI)

Either an SR PLDLA 96/70 composite plate or PDS folio was placed in the dorsal subcutaneous tissue of each animal. At the end of each follow-up a full thickness of dorsal skin containing the implant and the surrounding capsule was excised from each animal. Connective tissue capsules enveloping the plates were removed for immunohistochemistry. The mechanical properties of the implants were analyzed.

4.1.3. Implants

Experimental study using the rabbit model (I)

The implants were manufactured from poly-L/D-lactide acid stereocopolymer 85/15 (SR PLDLA 85/15), (Table 3). The self-reinforcing technique was used. The polymer was melt extruded at 135°C into circular rods of diameter 5 mm using an Axon BX-15 extruder (Axon, Sweden) and subsequently drawn at 90°C through a heated conical die to a draw ratio of 2.5. The drawn rods (diameter 3.8 mm and length 60 mm) were compressed between flat metal surfaces at 115°C using a 100 kN compression force to produce plates of thickness 0.3 mm. The plates were cut to a width of 12 mm and to a length of 50 mm. The mid-portion was perforated. The plates were then divided into two groups and sterilized either with gamma irradiation (2.5 MRad dose, g.i.) or with gas (ethylene oxide, e.o.).

Experimental study using the sheep model (III)

The implants were manufactured from low monomeric poly-L/D-lactide acid stereocopolymer 96/4 (SR PLDLA 96/4), (Table 3). The self-reinforcing technique was used. The polymer was melt extruded into continuous plates of thickness 0.45 mm ± 0.05 mm and width 80 mm using an Axon BX15 extruder (Axon, Sweden) equipped with a flat film die and an Axon BDB take-off machine. The SR PLDLA 96/4 plates were allowed to cool at room temperature (20^{o}C). After cooling the plates were reheated to 70°C and biaxially stretched into the shape of a bowl over a hemispherical steel die with a radius of 35 mm. After cooling, implants of diameter 28 mm were cut.

Micro tacks were manufactured using a self-reinforcing technique (SR) from the same poly-L/D-lactide acid stereocopolymer as the plates, at the Institute of Biomaterials, Tampere University of Technology, Tampere, Finland. Tacks, 5 mm long with a shaft of diameter 1.1 mm and a head of diameter 3.1 mm, were produced.

Experimental study using the rat model (IV)

The materials used were standard 0.25 mm x 30 mm x 40 mm orbital floor polydioxanone (PDS®) folio and a similarly shaped SR poly-L/DL-lactide copolymer composite implant (Table 3). P(L/DL)LA 70/30 (PLA70, i.v. 5.7 dl/g, Boehringer Ingelheim, Germany) was melt-extruded to thin, rigid plates (nominal thickness 0.3 – 0.4 mm). P(L/D)LA 96/4 (PLA96, i.v. 6.83 dl/g, Purac biochem b.v. Holland) was melt-spun to 4-ply multifilaments to a draw ratio 4.3.

Each SR PLDLA 96/70 consisted a mesh sheet (SR P(L/D)LA 96/4) compressed onto copolymer frame (SR P(L/DL)LA 70/30), (Figure 4). The self-reinforcing technique was used. Dimensions of the central area were 20 mm x 10 mm x 0.5 mm and the outer dimensions were 30 mm x 22 mm x 0.5 mm.

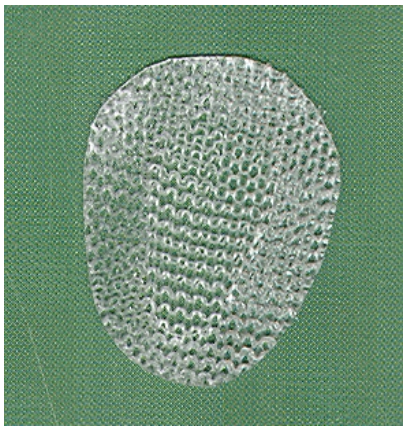

Figure 4.
Rat model: the shape of the SR PLDLA 96/70 implant was oval and composed of a mesh sheet centre within a solid frame.

4.1.4. Macroscopic evaluation and radiographics

Experimental study using the sheep model (III)

The macroscopic outcome of orbital floor reconstruction was evaluated by measuring both the largest residual bone defect and the deepest depression of the orbital floor under the direct vision using a calliper ruler.

The specimen was placed on a standard X-ray unit plate and fixed to the chin rest (Scanora, Soredex, Orion Corp., Helsinki, Finland) with the orbital floor horizontal. Narrow beam linear scanning (60 kV, 4 mA, 16 s, magnification factor 1.2) and spiral (=multidirectional) tomography (60 kV, 1.6 mA, 4 x 20 s, magnification factor 1.2) with 4 mm cuts were used. For narrow beam linear scanning, each specimen was imaged separately. For tomography, left and right orbital specimens were placed side by side.

Orbital depression was measured in both images of every specimen and expressed in mm (corrected by the magnification factor). New bone formation was evaluated by measuring the thickness of bone in the defect area. This is expressed in millimetres, measured perpendicular to the orbital floor.

4.1.5. Material characterization

Experimental study using the rabbit model (I)

The changes in tensile strength and crystallinity, and changes in intrinsic viscosity (indicative of molecular weight) were determined.

The tensile strengths of the intact plates and after *in vivo* exposure were measured using a Lloyd 6000R Materials Testing Machine (Lloyd Instruments PLC, Fareham, UK) at room temperature (22-23°C). The cross-head speed was 10 mm/min and the gauge length 20 mm.

The degree of crystallinity was estimated from the heat of fusion, assuming 93.7 J/g calculated by Fischer and coworkers (1973) for 100% crystalline PLLA. Duplicate samples were used. A Perkin-Elmer DSC-7 differential scanning calorimeter (DSC, Perkin-Elmer Co., USA), calibrated with indium standards, was used to determine the heat of fusion of intact SR PLDLA 85/15 plates and after *in vivo* exposure. The DSC was operated at a heating rate of 20°C/min. Dry 6 ± 1 mg samples evacuated at room temperature for 3 days were used in each case. The samples were heated in a nitrogen atmosphere from room temperature to 200°C and the heat of fusion was estimated from the area enclosed by the DSC curve and the baseline.

The viscosity values (according to ASTM D 445-88) of the plates equivalent to the molecular weight of the polymer were measured in chloroform at 25°C with an Ubbelohde capillary viscometer. Inherent viscosities in a 0.1% (0.1 g/dl) solution were determined as an indication of molecular weight decrease during degradation (Pistner *et al.* 1993). Viscosity-average molecular weights (g/mol) were estimated using the Mark - Houwink equation (Gogolewsky *et al.* 1993).

Experimental study using the sheep model (III)

The shear strength of the plate was determined by shearing a 6 mm diameter hole through the plate using a punching tool assembly constructed to a modification of BS 2782, method 340 A. The test was performed at 20°C in a Lloyd 6000R material testing machine (Lloyd lnstruments, PLC, UK) operating at a cross-head speed of 10 mm/min. Shear strength was calculated from the following equation: S = F/лDT (S =shear strength (MPa), F=force (N) at fracture, D=diameter (mm) of punch, T=mean thickness (mm) of plate).

The degree for the crystallinity and the viscosity values were measured using the methods described for the rabbit model (I) above.

Experimental study using the rat model (VI)

Gel Permeation Chromatography (GPC)

Each sample was weighed to 7.35 ± 0.15 mg. The mesh, the frame and PDS were analysed separately.

The weight-average molecular weight (M_w) and polydispersity (PD) values of the samples were determined. PLDLA samples were dissolved in chloroform and incubated for 24 hours at 22°C. 5 µl of 6% dichlorobentzene was added to each sample to provide a reference peak. Two parallel samples were used. Two Mixed-C columns (Polymer Laboratories, MA, USA) and one primary column (Polymer Laboratories) were used. The GPC system consisted of Waters 410 RI (Waters, Milford, MA, USA) differential refractometer detector and a Waters 515 high-pressure liquid chromatography (HPLC) pump. Chloroform was both eluent and solvent. The injected sample concentration was 0.1 mass-% and, the injection volume and eluent flow rates were 150 µl and 1 ml/min respectively. PDS samples were dissolved in chloroform and then incubated overnight at 45°C. Further procedures for PDS samples were as described above for the P-L/DL-LA samples.

The analysis was carried out using Millenium 32 software.The mathematical definition of weight-average molecular weight (M_w) is shown by the following formula:

$$\overline{M}_w = \Sigma(N_i M_i^2) / \Sigma(N_i M_i)$$

where Ni is the number of molecules with molecular weight Mi.

Polydispersity (PD) is the ratio of weight-average molecular weight to number-average molecular weight:

$$PD = \overline{M}_w / \overline{M}_n$$

where PD is polydispersity, and M_w is the weight-average molecular weight. PD indicates the width of the distribution.

Differential Scanning Calorimetry (DSC)

Each sample was weighed to 6 ± 0.1 mg. The frame (P(L/DL)LA 70/30), the mesh sheet (P(L/D)LA 96/4) and PDS were analysed separately.

The glass transition temperature, melting temperature and crystallinity of the samples were determined using a Perkin Elmer Pyris 1 DSC Differential Scanning Calorimeter (Perkin Elmer Instruments, Norwalk, CT, USA). An automated sampler, Autosampler (Perkin Elmer Instruments), was used. The equipment was indium calibrated and results were calculated using the baseline. Experiments were performed in a nitrogen atmosphere. Each polylactide sample was heated from 27°C to 220°C at 20°C/min and then rapidly cooled to 27°C at 200°C/min before the heating cycle was repeated. Each PDS sample was heated from – 40°C to +140°C at 20°C/min and then rapidly cooled to – 40°C at 200°C/min before the heating cycle was repeated.

The results were analysed using a Perkin Elmer Analyser program (Perkin Elmer Instruments, Norwalk, CT, USA). T_g was determined from the second heating cycle, i.e. after rapid cooling the extrapolated value provided by the analysis program was used. T_m and crystallinity were determined from the first heating cycle. The crystallinity of PDS was determined by assuming the initial value of crystallinity to be 100. The values obtained for the following samples were then compared with this value.

4.1.6. Histology and immunohistochemistry

Experimental study using the rabbit model (I)

Indirect immunofluorescence was performed with cryosections of 5 μm thickness. The specimens were incubated in the primary antibodies for 30 min, tenascin (Howeedy *et al.* 1990) and cellular fibronectin (Vartio *et al.* 1987), (Table 4.) before addition of fluorescein isothiocyanate (FITC)-coupled sheep anti-mouse IgG antiserum (dilution 1/120, Sigma, St Louis, MO, USA). The stained sections were coated with glycerine (dilution 3/1 with phosphate-buffered saline). The sections were examined in a Leica Aristoplan.

The degree of immunofluorescence staining was evaluated by two observers independently using 100 - 200 x magnification by means of an arbitrary scale (– = no or slight reactivity, + = moderate or high reactivity).

Table 4.
Rabbit model. Antibodies used for immunohistochemistry
[1]Sigma, St Louis, MO, USA

Antigen	Antibody	Source	Negative control
Tn	100 EB2	I. Virtanen	Normal mouse serum
cFn	52 DH1	I. Virtanen	Normal mouse serum
α-actin	Mouse monoclonal antibody	Sigma[1]	Normal mouse serum

Experimental study using the sheep model (III)

Frozen sections 6 μm thick were used for hematoxylin and eosin staining and for APAAP immunohistochemistry (Dako A/S, Glostrup, Denmark). Sections were first incubated in primary antibodies for tenascin (Balza *et al.* 1993) and cellular fibronectin (Vartio *et al.* 1987), (Table 5.). Secondary antibody was applied for 30 minutes before counterstaining in Mayer dye.

The degree of immunostaining was evaluated by two observers independently using 40x magnification by means of an arbitrary scale (– = no reactivity, + = moderate or high reactivity). Four consecutive visual fields (0.23 mm x 0.16 mm) were evaluated.

Table 5.
Sheep model. Antibodies used for immunohistochemistry

Antigen	Antibody	Source	Negative control
Tn	BC-2, BC-4	L. Zardi	Non-immune serum
cFn	52 DH1	I. Virtanen	Non-immune serum

Experimental study using the rat model (VI)

Indirect immunofluorescence staining was performed on 5 μm thick cryosections. Sections were first incubated in primary antibodies for Tn-C (1:250) and α-actin (1:400) followed by fluorescence isothiocyanate (FITC)–conjugated sheep anti-mouse IgG (1:250) for Tn-C, rodamine-conjugated goat anti-rabbit (1:100) for α-actin and DAPI (1:200) for cell nucleus (Table 6). Sections were examined with a Leitz Aristoplan microscope (Leitz, Wetzlar, Germany) with an epi-illuminator and appropriate filters.

T-lymphocyte marker CD2 and type I collagen were stained using an ARK™ manual Animal Research Kit (Dako, Glostrup, Denmark). The antibodies are listed in Table 6. Type III collagen was stained using a Vectastain® ABC manual Avidin-Biotin Peroxidase Complex method kit (Vector Laboratories Inc., CA, USA). During type III collagen staining, sections were incubated with a collagenase C6885 (Sigma, St. Louis, MO, USA) solution.

Endogenous peroxidase-positive monocytes/macrophages were detected using endogenous peroxidase staining.

Table 6.
Rat model. Antibodies used for immunohistochemistry
[1]Telios Pharmaceuticals, San Diego, CA, USA
[2]Serotec Ltd.,Oxford, England
[3]Chemicon International, Inc., CA, USA
[4]Calbiochem-Novabiochem Corp., CA, USA

Antigen	Antibody	Source	Negative control
Tn-C	Rabbit polyclonal immunoglobulin	Telios[1]	Non-immune serum
α-actin	Rabbit monoclonal antibody	Telios[1]	Non-immune serum
CD2	Mouse monoclonal IgG CD2	Serotec[2]	Non-immune serum
Collagen I	Monoclonal collagen I antibody	Chemicon[3]	Dako X 0931
Collagen III	Polyclonal immunoglobulin	CN[4]	Dako X 0903

4.1.6. Electron microscopy

Experimental study using the rabbit model (III)

Transmission electron microscopy (TEM)

For electron microscopy, a small fragment of connective tissue was cut. These fragments were fixed in 2% glutaraldehyde in phosphate buffer (0.1 M, pH 7.4) for 60

minutes and postfixed in 1% osmium tetroxide in the same buffer. After dehydration, the specimens were embedded in Epon 812. Thin sections (1 μm) were cut and stained with methyl blue and studied under a stereomicroscope for orientation. Ultra-thin sections were then made of representative specimens stained with uranyl acetate and lead citrate and studied in a Jeol 1200EX transmission electron microscope (Jeol Ltd, Tokyo, Japan) operating at 60 kV accelerating voltage.

Experimental study using the rat model (VI)

Scanning electron microscopy (SEM)

The implants comprising mesh sheet and the frame PLDLA 96/70 and PDS were cut with a surgical blade and glued with conductive graphite (Pelco ® Conductive Graphite, Pelco International, Redding, CA, USA) onto a metal mount, dried for 2 hours in a laminar flow hood and then overnight in vacuum at room temperature. The samples were coated with gold in an Edwards S 150 Sputter Coater (BOC Edwards, MA, USA) for 90 seconds twice at 20 mV in an argon atmosphere. The samples were analysed using a JEOL T100 scanning electron microscope (Jeol Ltd, Tokyo, Japan) at 15 kV with SemAfore (Jeol Ltd.) analysing program.

4.1.8. Statistics

Experimental study using the rat model (VI)

The analysis of tenascin and α-actin reactivity was qualitative. An arbitrary scale, 0 = no or slight reactivity, 1 = moderate or high reactivity, was used. Stained sections were compared with control sections from which primary antibody had been omitted.

The analysis of cell densities of T-cell and monocyte/macrophage was quantitative and was performed using a stage micrometer (Graticules Ltd, Tonbridge, Kent, England). The area of each rectangle was of 0.0368 mm^2 (dimensions: 0.23 x 0.16 mm^2). The number of positively stained cells in four parallel rectangular areas was counted for all animals, from the implant surface towards the dense connective tissue. The cell density (cells / mm^2) was calculated by dividing the average number (N=3) of detected cells with area examined.

Type I and type III collagens were quantified using a 10 x 10 ocular grid (Zeiss, Esslingen, Germany). Five random ocular grid areas from each zone (inner layer / outer layer) in all samples (N=3) were analyzed. Positively stained squares were calculated

and the results were given as the percentage of positive squares per 100 squares (10 x10 grids). The results are presented as an average (N=3).

Statistical differences between T-cell and monocyte/macrophage densities (PDS vs. SR PLDLA 96/70) and between collagen I and III positivities (PDS vs. SR PLDLA 96/70 and inner vs. outer layer) were tested using student's t-test. The data tested was normally distributed.

The statistical differences between T-cell and monocyte/macrophage densities and type I and III collagen positivities as a function of time were tested using the nonparametric Kruskall-Wallis test.

Statistical tests were performed using GraphPad Prism ® software (GraphPad Software, Inc. 5755 Oberlin Drive, #110 • San Diego, CA 92121 USA).

4.2. Clinical studies (II, IV)

Clinical studies included two different models, one using bone graft (IV) and the other polydioxanone (PDS®) folio (II) as implant material. Twenty-four consecutive orbital blowout fractures were reconstructed using autogenous iliac bone grafts and 16 consecutive orbital blowout fractures using PDS® folio (Ethicon, Johnson & Johnson, Brussels, Belgium). This study was approved by the local ethical committee.

4.2.1. Implants

The free bone graft was harvested from the medial wall of the anterior ileum and trimmed with a drill bit to cover the defect being measured. The thickness of the graft was thinned down to 1 mm in the periphery and to 2-3 mm in the central area.

PDS implants of two different shapes and sizes were used. They were either kidney shaped folios of 40 mm x 30 mm x 0.25 mm or round plates of 28 mm x 1 mm. The former were used in six patients and the latter in nine. One patient was treated with both.

4.2.2. Operative techniques

The orbit was explored by approach through subciliary or lower eyelid. The periost was sharply incised at the infraorbital rim and the fracture area was exposed. The prolapsed orbital content was repositioned. The orbital floor was reconstructed using either a subperiosteally placed iliac crest graft or a PDS implant.

4.2.3. Clinical examinations

The study protocol consisted of clinical examinations preoperatively and at 1, 2, 4, 8, 16, 36 (bone graft) and at 1, 2, 4, 8, 12, 36 (PDS) weeks postoperatively. During each follow-up, eye movements in nine directions, enophthalmos and hypo-ophthalmus were assessed. The degree of horizontal displacement was measured using a Keeler exophthalmometer®. Vertical displacement was measured using an optician's examination spectacles provided with a vertical scale calibrated in millimetres.

4.2.4. Computed tomography and magnetic imaging

CT and MRI imaging were performed preoperatively, and 2 weeks, 30 weeks (iliac crest graft) and 36 weeks (PDS) postoperatively.

The CT examinations were performed using a Siemens Somatom CR CT scanner (Siemens, Erlangen, Germany) with 4 mm thick contiguous slices in the coronal and sagittal planes. The scan parameters were: voltage 125 kV, MAS 500, measuring time 7 s, projections 720.

MRI was performed using a Siemens Vision imager operating at 1.5 T (Siemens, Erlangen Germany). Coronal slices perpendicular to the optical nerves were obtained from both eyes with a T1-weighted spin-echo (SE) sequence 600/15/3 (TR/TE/excitations). Coronal T2-weighted fat suppression sequence 1800/20/1/150 (TR/TE/excitations/FA) of the fractured internal orbital wall was obtained in all patients. T1-weighted slices were 2 mm thick with a 0.2 mm interslice gap. T2-weighted slices were 3 mm thick with a 0.3 mm interslice gap.

The angle and position of the *in situ* iliac bone graft were assessed using CT imaging in the following manner: the angle was assessed by comparing the sagittal and coronal plane of the bone graft with that of the floor of the uninjured orbit. If the angle was identical it was graded good, otherwise poor. The craniocaudal height of the bone graft was measured at both anterior and posterior orbits using the uninjured orbital floor as the theoretical reference plane. The difference was measured in millimetres by comparing the position of the bone graft with the floor of the uninjured orbit; minus (-) stands for caudal and plus (+) for cranial direction. The state of resorption was assessed qualitatively and graded as follows: 0 = total, 1 = moderate, 2 = mild, and the state of bone growth: 0 = none, 1 = moderate, 2 = intense.

4.3. Finite element analysis (VI)

Geometric modelling and material properties

The bony orbit was approximated as a pyramid with the base serving as an opening for the eye and the apex directed towards the brain (Power 2001, Sauerland 1994). The height of the pyramid was approximately 50 mm, while the opening for the optic nerve was approximately 10 mm. The bone was simulated as an orthotropic material and its elastic properties were derived from past reports (Table 7). The model of the human eye was composed of a superficial layer formed by the cornea and sclera and inner layer formed by the lens, held in place by ciliary and vitreous bodies and aqueous humour. For simplicity, the cornea was assumed to be spherical, with a central thickness of 0.5 mm and a central radius of curvature of 7.8 mm (Uchio *et al.* 2001, Uchio *et al.* 2003). The material properties of the several components of the eye are summarised in Table 7 and taken from a study by Uchio and coworkers (2001). The lens was modelled as a rigid body, and the vitreous body as a solid mass with a hydrostatic pressure of 20 mm Hg (2.7 KPa). The cornea was loaded by the intra-ocular pressure on the posterior surface and by atmospheric pressure on the anterior surface. The loading produced by the eyelids was ignored (Kobayashi *et al.* 1971, Uchio *et al.* 2001). The finite element model was loaded using multiple force vectors to simulate muscle forces.

Table 7.
Summary of eye's material properties. E: Young′s modulus of elasticity. ν: Poisson′s ratio. The first subscript is the direction of the primary strain, the second subscript is the direction of the secondary strain.

STRUCTURE	YOUNG′S MODULUS E (MPa)	POISSON′S RATIO (ν)	DENSITY (kg/m^2)	LITERATURE SOURCE
Cornea	Nonlinear	-	1400	Uchio 2001
Sclera	Nonlinear	-	1400	Uchio 2001
Extra/ocular muscles	11.0	0.40	1600	Power 2001
Ciliary body	11.0	0.40	1600	Power 2001
Fatty tissue	0.047	0.49	999	Power 2001
Vitreous body	0.042	0.49	999	Power 2001
Aqueous body	0.037	0.49	999	Power 2001
Lens	-	-	315	Power 2001
Bone	$E_x = 19.5$ $E_y = 13.6$ $E_z = 10.2$	$\nu_{xy} = 0.39$ $\nu_{yz} = 0.20$ $\nu_{xz} = 0.55$	-	Dechow *et al.* 1992

Finite element modelling (FEM)

The geometric entities created in the previous step were mapped with finite elements and nodes. Mapping was performed with the semi-automatic option Finite Element Generation (FEG) available in Display III (NISA, EMRC, Troy, USA). The mesh volumes of the bony orbit, vitreous and fatty tissues were subdivided into brick-shaped (six sided with 24 degrees of freedom) and wedge-shaped (five sided with 18 degrees of freedom) solid linear elements. Triangular membrane elements were used to model the cornea and sclera. To maintain a proper geometrical aspect ratio, thin regions were subdivided into an extremely high number of elements. When the solid parabolic brick elements were used to model such a complex shape as that of the orbit, it has been noted that although more degrees of freedom would give better interpolated data, the mid-side nodes of the elements also allow for higher distortions to occur (Korioth and Versulis 1997, Al-Sukhun 2003). Thus, by selecting a higher number of less distorted solid linear brick elements, the orbit was expected to be satisfactorily modelled. The finite element model was checked for node coincidence and discontinuities (i.e. gaps between elements).

A typical missile impact velocity of 30 m/s was used in this study. In view of the clinical data, the range of missile weight in this simulation was set at 0.5 ─ 1 kg. The impact was initially directed at right angles from the front to the orbital rim. The simulation was performed five times, with the direction of the missile impact varied by 45^0 upward, downward, right and left. The finite element model was then used to predict the variables at each node position. These variables were:

1. Stresses / Strains - in the form of maximum, minimum and shear stresses / strains
2. Displacement - representation of motion of structures.

5. RESULTS

5.1. Experimental studies (I, III, VI)

5.1.1. Macroscopic findings

Experimental study using the rabbit model (I)

SR PLDLA 85/15 implants were broken already at week 4 (Figure 5). At week 48, macroscopic examination revealed that the gamma-sterilized implants had disappeared whereas the ethylene-oxide sterilized implants were seen as rounded masses.

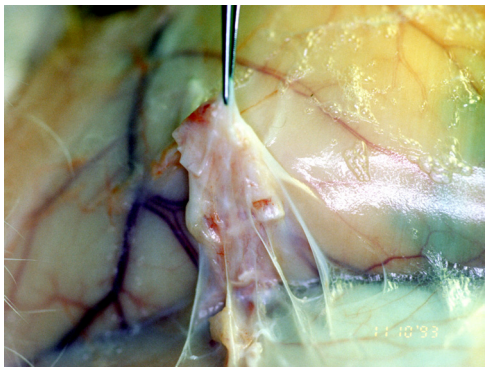

Figure 5.
Rabbit model: SR PLDLA 85/15 implants were removed from the dorsal subcutaneuos tissue together with the surrounding connective tissue capsule. Note the fractured SR PLDLA 85/15 plate.

Experimental study using the sheep model (III)

At week 12, all five SR PLDLA 96/4 implants were considerably deformed and coiled (Figures 6 - 7) and enveloped in a thick and elastic connective tissue capsule. Originally pliable implants had become fragile. A residual defect in the bone was seen in 6 out of 10 of the orbital floors, equally the reconstructed and control sides. All reconstructed orbital floors were mildly (5-7 mm) displaced into the maxillary sinus.

At week 36, three implants were surrounded by a bony capsule. The shape of the implant was identical to the shape of the displaced (sunken) orbital floor. Two capsules contained fluid. Clinical examination of the specimen showed that fractured orbital floors had healed and bony union was achieved (Figures 8 A and B). However, the correct positions of the orbital floors were not achieved.

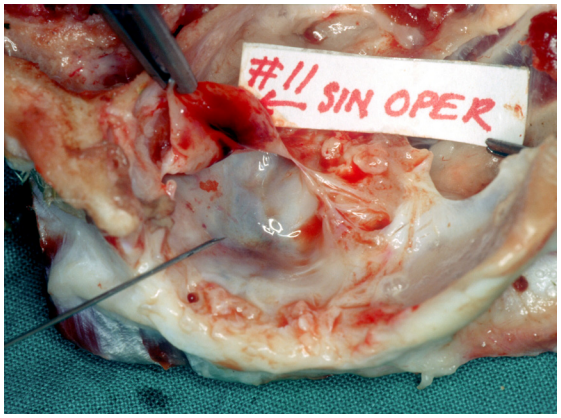

Figure 6.
Sheep model: SR PLDLA 96/4 implants were identified and removed after separating the orbits from the skull. The implant capsule is elevated and is shown here by a needle.

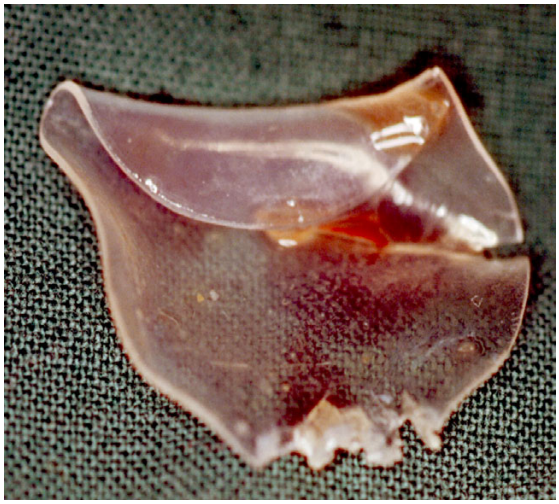

Figure 7.
The SR PLDLA 96/4 implants were deformed after only 3 months without any macroscopic signs of degradation.

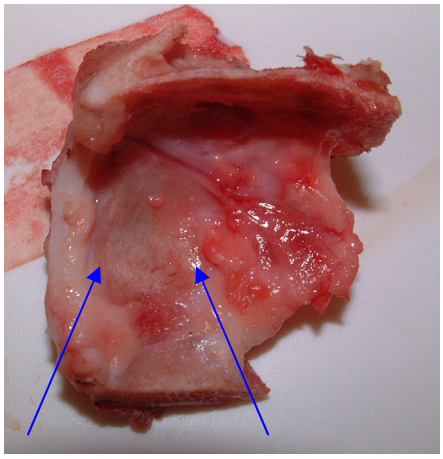

Figure 8 A.
After removal (9 months) of the SR PLDLA 96/4 implant bone growth over the defect area (arrows) was detected.

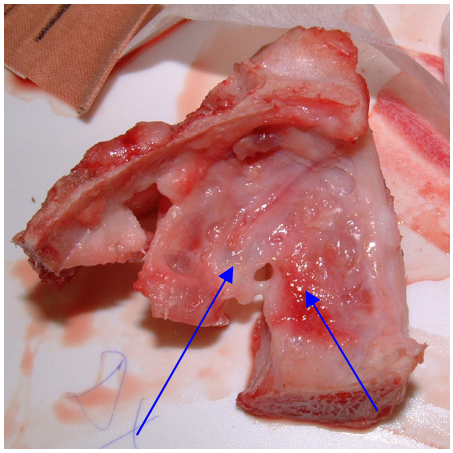

Figure 8 B.
On the control side a residual defect (arrow) was macroscopially visible in only one case.

Experimental study using the rat model (VI)

Primary healing was good in all animals except one in the PDS group, which suffered superficial wound dehiscence. However, this healed well during the first week of observation.

After two months the PDS folio had degraded into hard, sharp pieces inside the thick capsule (Figure 9.). After three months the PDS had degraded further, but no changes in the PLDLA 96/70 implants were apparent. After four months the PLDLA 96/70 implants were about the same size as at the beginning but had acquired the shape of the dorsum. No further change in shape was observed. After five months the PDS implant had become a soft, round mass with a maximum diameter of 10 mm.

Figure 9.
Rat model: SR PLDLA 96/70 and PDS® implants were removed from the dorsal subcutaneus tissue with the surrounding connective capsule. The degrading PDS implant is encapsulated, the capsule is thick and clearly visible.

5.1.2. Radiographic findings

Experimental study using the sheep model (III)

Coronal CT sections from the specimen showed that bone defects did not ossify during the study. The differences in the size and shape of the defect between the implant and control groups were not statistically significant. A discrepancy was seen between results of CT imaging and the results of the clinical observation (Figure 10).

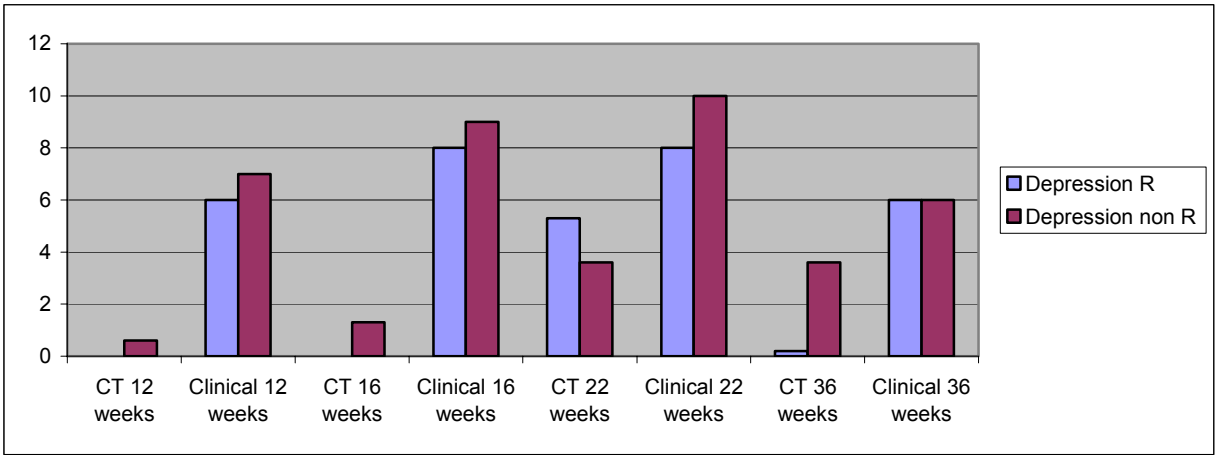

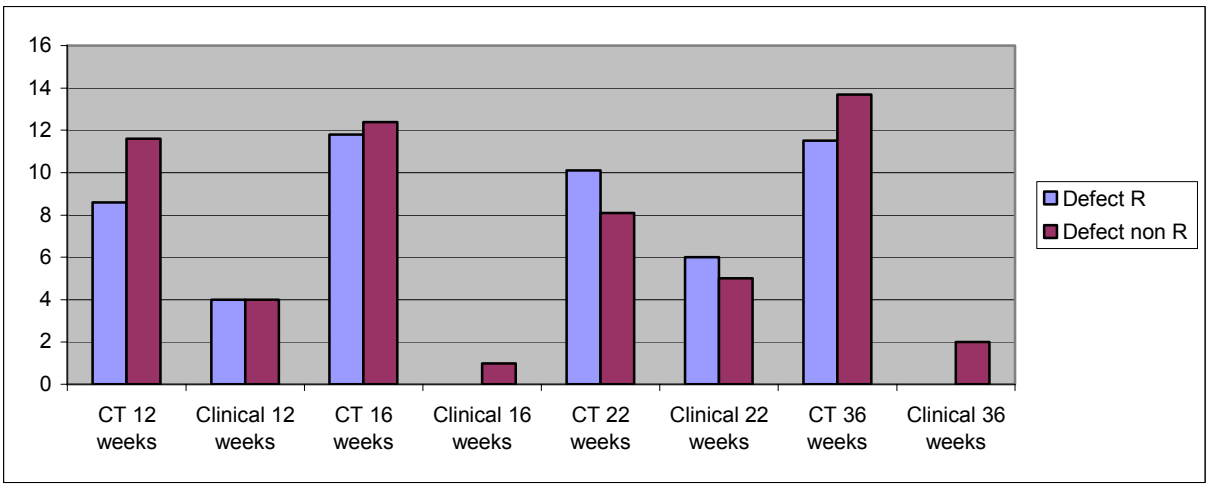

Figure 10.
The bone depressions and defects of reconstructed (SR PLDLA 96/4 implant) orbital floors measured by CT imaging and clinically, from both reconstructed (R), and non-reconstructed sites (non R). No statistical differences were found between the two groups. Note the discrepancy between clinical and CT results. Results are average values in mm.

5.1.3. Strength and crystallinity findings

Experimental study using the rabbit model (I)

The SR PLDLA 85/15 implant was inadequate, as it had already broken by week 4. The initial tensile strength was 43.8 MPa for ethylene oxide-sterilized and 33.1 MPa for gamma-irradiated implants. Tensile strengths could not be measured because of the implants' fragility. The initial mean M_v molecular weights for e.o. and g.i. implants were subsequently 61050 and 38480 g/mol. During the 16 weeks follow-up, the

molecular weights decreased to 27 560 and 12730 g/mol, respectively. At the same time, the crystallinity increased in both e.o. and g.i. groups.

Experimental study using the sheep model (III)

The plates had an initial shear strength of 107.2 ± 14.8 MPa. At week 16, the shear strength had decreased to 78.2 ± 15.4 MPa. Subsequently the shear strength could not be measured because of the fragility of the material. Because of processing and gamma irradiation the inherent viscosity of the plate material was 1.44 dl/g although that of the raw material had been 8.27 dl/g. Inherent viscosity decreased with implantation time to 0.64 dl/g in 16 weeks and to 0.24 dl/g in 36 weeks. On the basis of enthalpy change, the initial crystallinity was 1.5%. Crystallinity increased steadily up to 29% at week 36. At the same time the molecular weight decreased from 48725 to 4186 g/mol (Figure 11 and 12).

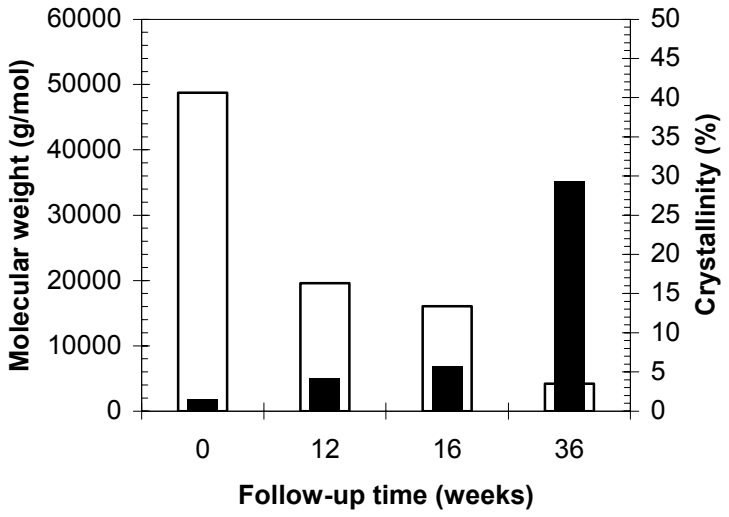

Figure 11.

Sheep model. Change in M_v molecular weight (white columns) and crystallinity (black columns) with time. Data characteristic of SR PLDLA stereocopolymers with an isomer ratio of 96/4.

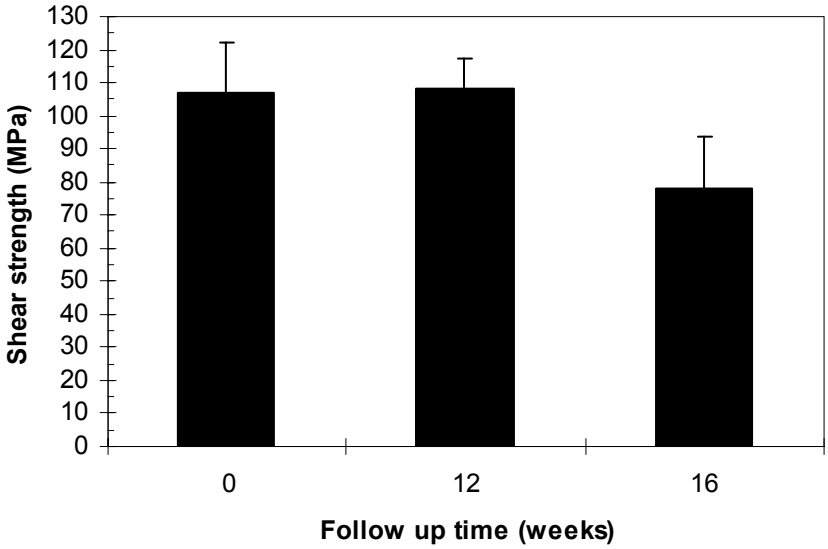

Figure 12.

Sheep model. Changes in shear strenght with time. Data characteristic of SR PLDLA stereocopolymers with an isomer ratio of 96/4.

Experimental study using the rat model (VI)

Gel Permeation Chromatography (GPC)

The molecular weights ($M_{w)}$ of P(L/D)LA 96/4 and P(L/DL)LA 70/30 are in Figure 13. The M_w and M_n of PDS (Figure 14) decreased by over 50% during the first month. The rate of decrease during the second month was very similar.

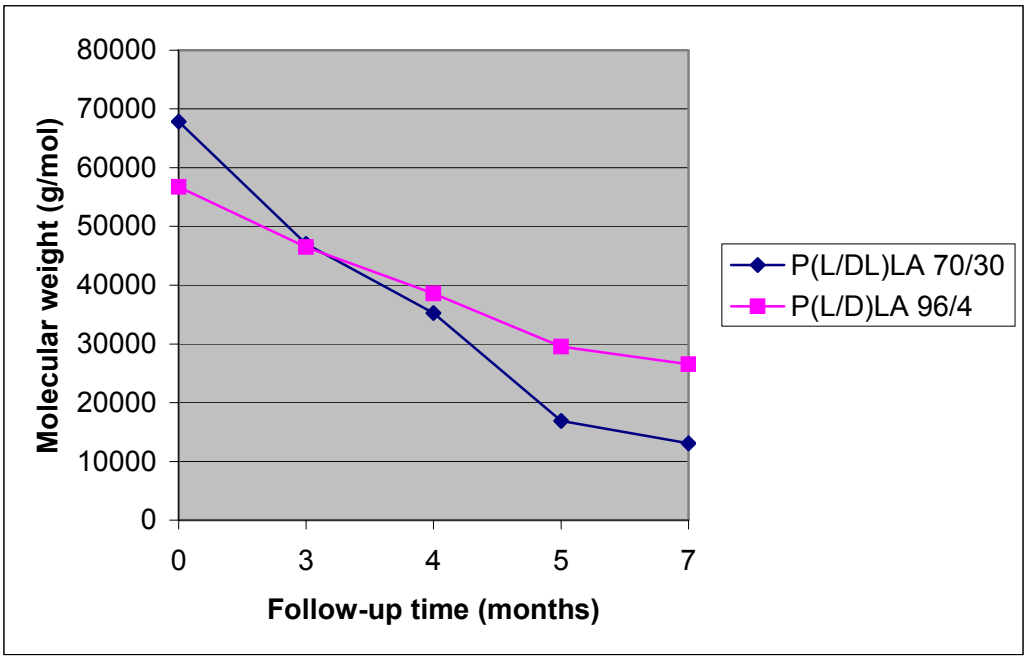

Figure 13.
Rat model. Changes in two components of the SR PLDLA 96/70 composite implant. Change in weight-average molecular weights (M_w) of SR P(L/DL)LA 70/30 and SR P(L/D)LA 96/4 material with time.

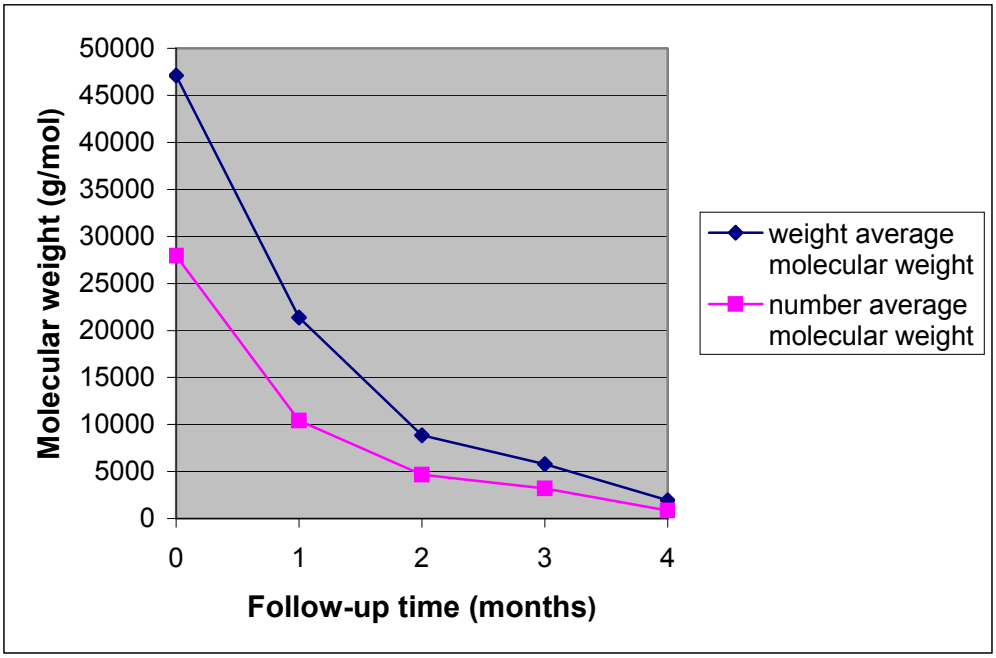

Figure 14.
Rat model. Changes in molecular weights (M_w and M_n) of PDS with time.

Differential Scanning Calorimetry (DSC)

Changes in the crystallinity of SR P(L/D)LA 96/4 and SR P(L/DL)LA 70/30 are shown in Figure 15. The crystallinity of the originally amorphous SR P(L/DL)LA 70/30 started to increase at month 5. By contrast, the crystallinity of SR P(L/D)LA 96/4 decreased. The T_m of SR P(L/D)LA 96/4 and SR P(L/DL)LA 70/30 varied *in vivo* but no increase or decrease was observed. However, T_g showed a decreasing trend over five months, followed by a slight increase. The pattern was similar with PDS, but the decrease continued for three months. The increase of crystallinity of PDS over time is shown in Figure 16.

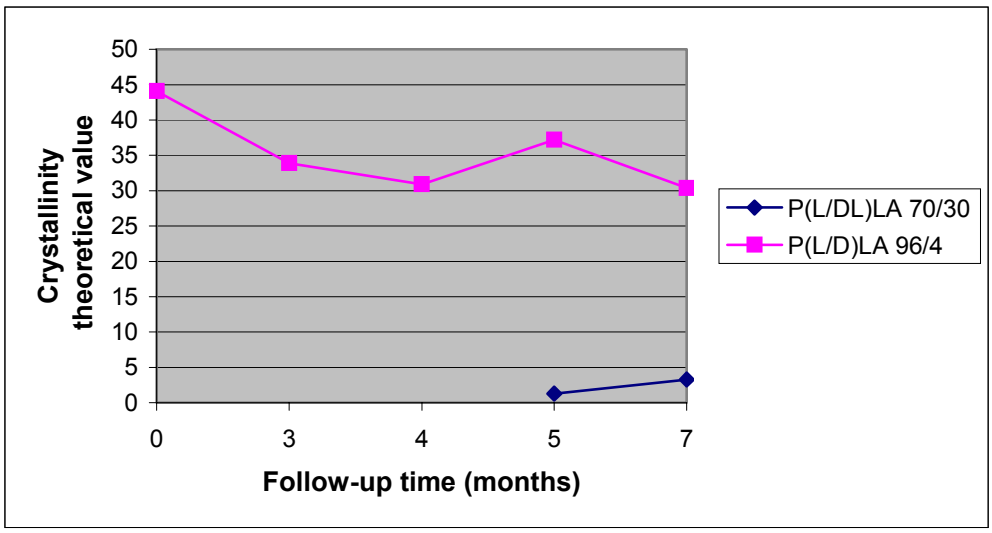

Figure 15.

Rat model. Changes in the crystallinity of two components of the SR PLDLA 96/70 composite implant. SR P(L/DL)LA 70/30 and SR P(L/D)LA 96/4 materials plotted against time.

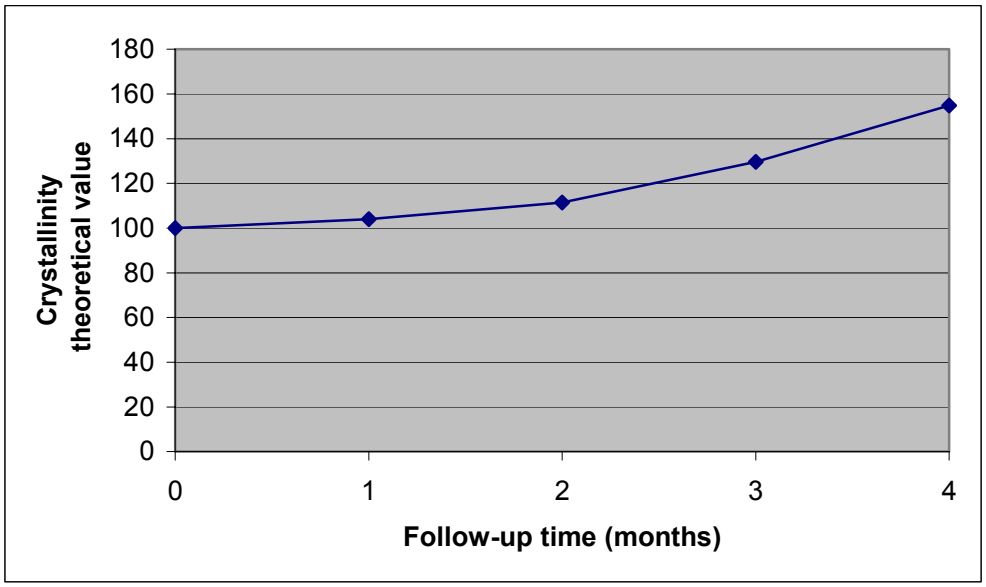

Figure 16.

Rat model. Relative changes in the crystallinity of PDS with time. The initial value is assumed to be 100.

5.1.4. Histology and immunohistochemical findings

Experimental study using the rabbit model (I)

All the SR PLDLA 85/15 implants were enveloped by a connective tissue capsule consisting mainly of fibroblast-like cells. Some macrophages, lymphocytes and

polymorphonuclear leukocytes were observed, suggesting a low-grade chronic inflammation. In 36 and 48 weeks specimens, pseudosynovial membrane-like tissue interfacing implants was detected. No differences were seen between capsules of the gamma-irradiated or ethylene oxide-sterilized implants.

During the first 36 weeks there was an intense reactivity for both tenascin and cellular fibronectin. An intense reactivity for cellular fibronectin and α-actin persisted to the end of the study around the implant material. Immunostaining of smooth muscle α-actin demonstrated a thick layer of activated myofibroblasts in areas presenting cellular fibronectin and tenascin immunoreactivities.

Experimental study using the sheep model (III)

At the week 12, the fibrous capsules around SR PLDLA 96/4 contained fibroblasts and inflammatory cells. The week 36 specimen showed fibrocartilagenous areas around all capsules.

Widespread reactivity for tenascin was detected in the connective tissue against implant surfaces on week 12 specimens. Cellular fibronectin was diffusely present in the connective tissue, and the pattern of immunoreactivity was comparable to that for tenascin. The reactivities for tenascin and cellular fibronectin became more restricted at weeks 22 and 36 and were observed in the immediate vicinity of the implant.

Experimental study using the rat model (VI)

The capsules around all three types of implant consisted of two zones: an inner, thin, cell-rich zone and an outer, dense, connective tissue zone containing a few fibroblast-like, spindle-shaped cells (Figures 17 A and B.).

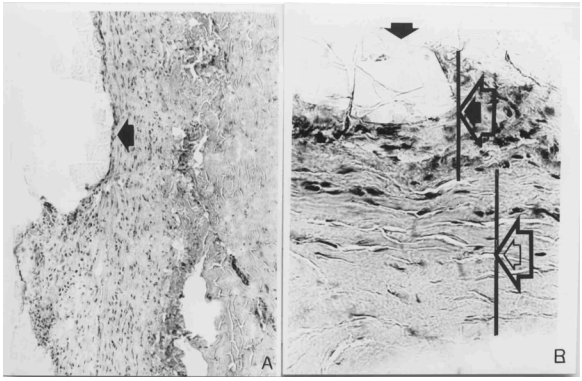

Figures 17 A and B.
Rat model: A thin cell-rich zone is detected on the surface of the implant.
Black arrow = implant; black arrow / large arrow = cell-rich inner zone; transparent arrow / large arrow = outer dense connective tissue zone.

After two months PDS fragments were in close contact with a thin inner zone containing numerous mononuclear cells and giant cells. At the 5 month follow-up, the capsules, which had earlier been found to consist of a single compartment, were divided by numerous thin walls. The changes in SR PLDLA 96/70 during follow-up were minor. Tenascin expression was local and restricted with both SR PLDLA 96/70 and PDS (Figure 18). Triple staining showed that tenascin expression occurred in the inner cell-rich zone near the implant surface. In contrast to tenascin, α-actin was present in dense connective tissue zones throughout the follow-up and formed belt-like structures around but a little apart from the degrading implants.

Figure 18.
Rat model: Immunofluorescence micro-graphs. Moderate amounts of tenascin around SR PLDLA 96/70 at month 7 (original magnification 400 x).

There was a highly significant difference ($P < 0.0001$) between type I and type III collagen positivity around all implants (Figure 19). Type III collagen expression in the inner zone was almost 20 times stronger than in the outer zone, whereas that of the type I collagen was exactly the opposite. However, there were no significant differences in type I and type III collagen positivities either between different follow-up times ($p>0.05$) or between PDS and SR PLDLA 96/70 ($p>0.05$) implant materials.

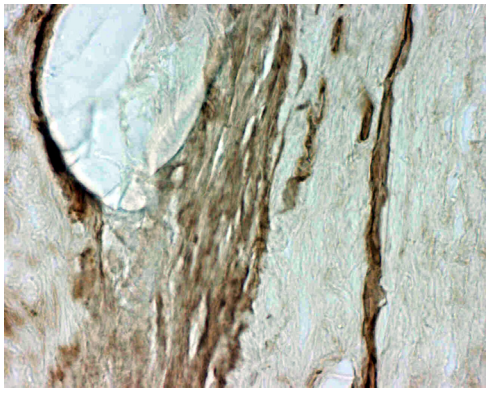

Figure 19.
Rat model. Note the clear difference in expression of type III collagen in the inner zone *vs.* outer zone of the capsule. SR PLDLA 96/70 implant, 7 months, type III collagen staining.

The T-lymphocyte density increased as a function of time around both materials but no statistically significant differences were found between PDS and SR PLDLA 96/70 ($p>0.05$) implants or between the inner and outer zones. Monocytes/macrophages showed an increase in density during the follow-up but no statistically significant differences were found. Both SR PLDLA 96/70 and PDS specimens followed the same pattern and no significant differences were found between them ($p>0.05$).

5.1.5. Transmission and scanning electron microscopy findings

Experimental study using the rabbit model (I)

In specimens examined by TEM the SR PLDLA 85/15 material were occasionally found to be surrounded by a layer of amorphous-like material.

Experimental study using the rat model (VI)

Degradation of the SR P(L/D)LA 96/4 and SR P(L/DL)LA 70/30 materials began to be visible in SEM at month 7. There were cracks in perpendicular direction to the long axis of the filaments. This was observed in the filaments of the SR P(L/D)LA 96/4 throughout the implant (Figure 20). This cracking was observed at the outer curve of the filament loop, where tension is the fracturing force.

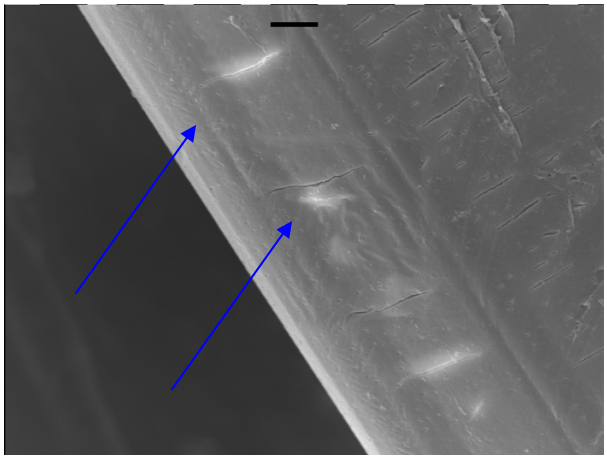

Figure 20.
Rat model. SEM image of SR P(L/D)LA 96/4 filament. Cracks (arrows) of perpendicular orientation at month 7. Scale bar 10 µm.

SR P(L/DL)LA 70/30 was also observed to have degraded strongly by month 7. The surface of the plate showed the same kind of changes in some parts and was detached from the porous core in some places (Figure 21). The surface layer of the material showed evidence of degradation.

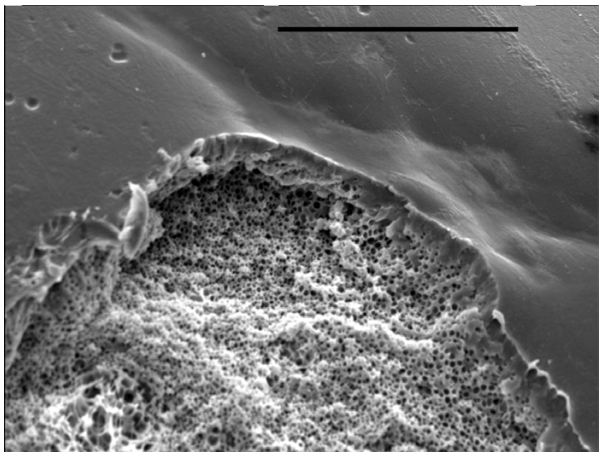

Figure 21.
Rat model. SEM image of SR P(L/DL)LA 70/30 plate surface. A fragment has detached from the surface and the inner porous structure is seen at month 7. Scale bar 100 µm.

PDS was also seen to have degraded strongly in the SEM observations. The degradation was observed as particles detaching from the PDS plates.

5.2. Clinical studies (II, IV)

5.2.1. Clinical results with the resorbable PDS implant (II)

Sixteen consecutive patients, 11 males and 5 females were included in this study. The mean age of the patients was 39.2 (18.0 - 58.9) years for men and 31.3 (20.1 - 53.2) years for women. The majority of the patients had been injured by interpersonal

violence (n=9 / 56%). Out of the 16 internal orbital wall fractures, ten were pure blowout fractures of the floor and six were associated with a nondislocated zygomatic fracture.

Preoperatively two patients (13%) had enophthalmos of more than 2 mm. The number of enophthalmic patients increased to six at the end of the study (Figure 22). The pattern of occurrence of hypoophthalmos was similar to the pattern of enophthalmos. There were no statistically significant differences between reconstructions using sheets or plates in relation to hypo-ophthalmos or enophthalmos.

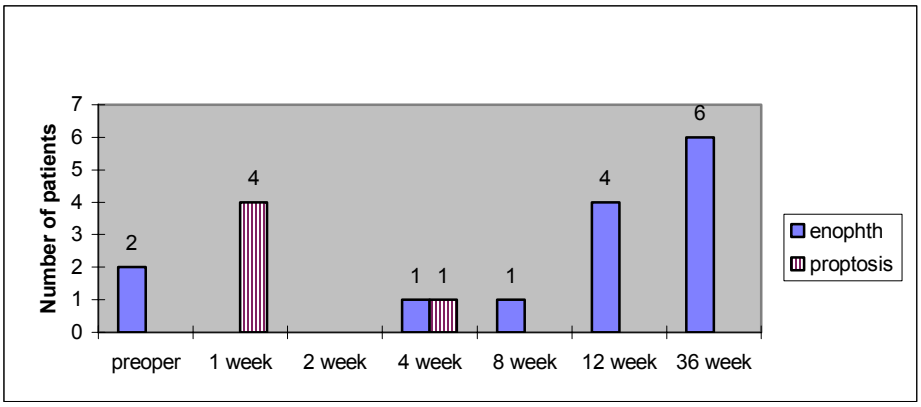

Figure 22.
Total number of patients with enophthalmos and proptosis of more than 2 mm during the clinical follow-up examinations after orbital floor reconstruction with PDS.

In one patient there was prolonged oedema in the lower lid region. At the 16th postoperative week, this patient developed an ipsilateral maxillary sinusitis with general symptoms. When the plate was removed several small PDS fragments were found inside the dense connective tissue capsule.

5.2.2. Clinical results with autogenous iliac crest graft (IV)

Twenty-four consecutive patients, 15 males and 9 females with unilateral orbital wall fractures were enrolled in the study. The mean age of the patients was 37.3 years (17.2 - 54.8 years). The main aetiology was assault (58%). Out of 24 patients 11 (46%) had pure orbital floor fracture and six (25 %) had an associated nondislocated zygomatic fracture.

Preoperatively, two (8%) patients had enophthalmos, and one (4 %) had hypo-ophthalmos of 2 mm or more. At the last follow-up, enophthalmos was detected in one

patient (4%, Figure 23), two (8%) had hyperophthalmos but five (21%) had hypo-ophthalmos.

Diplopia was registered preoperatively in 18 patients (75%). At the last follow-up, none of the patients presented diplopia in the central field of vision. The restrictions in eye movement resolved themselves and at the end of the follow-up no one had clinically detectable restrictions. However, 10 patients (42%) reported a subjective feeling of double vision in some direction of gaze.

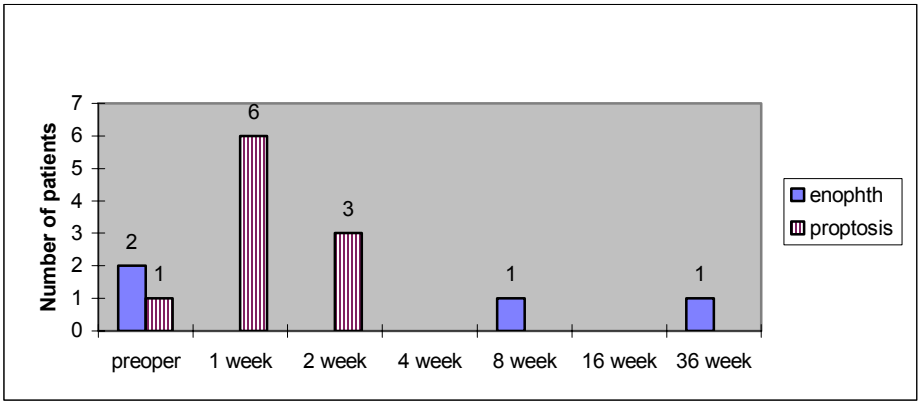

Figure 23.
Total number of patients with enophthalmos and proptosis of 2 mm or more during each clinical follow-up after iliac crest graft floor reconstruction.

One patient with medial wall and floor fracture was operated on twice. After the first operation, the globe was 2 mm proptotic but 3 mm hypo-ophthalmic. He was reoperated on and at the one-week follow-up the globe was slightly enophthalmic and hypo-ophthalmic. After eight months, the position of the globe had again deteriorated with 3 mm hypo-ophthalmos and 2 mm enophthalmos.

5.2.3. Radiographic findings

Resorbable PDS (II)

CT confirmed bone growth in the orbital floor, but new bone formation was detected in the fractured area, *i.e.* along the fractured floor, but not in the area where the PDS bridged the defect. As a consequence, the fractured floor on the final CT scan was similar to that seen on the CT taken before operation, and no repositioning of intraorbital tissue could be seen as a result of the plate. No long-term reduction in orbital volume therefore occurred (Figure 24). In one patient a possible orbitonasal fistula without clinical symptoms was observed at 13 weeks follow-up.

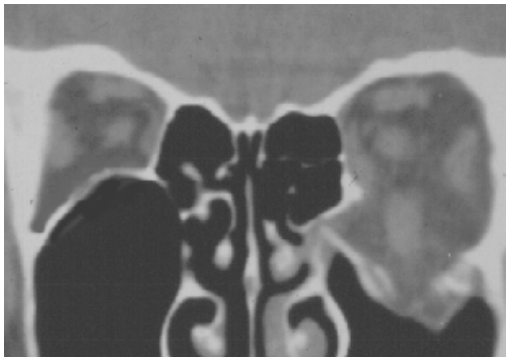

Figure 24.
PDS reconstruction. CT image 36 weeks postoperatively, volume and shape of orbit have not been restored.

No clear muscle herniations (entrapment) within the fracture area were observed in MRI or CT studies. The inferior rectus muscle was always surrounded by thick orbital fat. MRI revealed adverse peri-implant reactions in 10 cases (63%). These peri-implant lesions were 8 mm in thickness and were situated in the area of the implanted plate. Only one of these lesions resolved itself totally during the study.

In the patient with prolonged oedema in the lower lid region and an ipsilateral maxillary sinusitis with general symptoms, CT and MRI confirmed a large cystic formation inside the orbit and phlegm retention in the sinus.

Autogenous bone graft (IV)

Bone grafts were visualized well by CT imaging. At one-week follow-up CT imaging demonstrated that the orbital floor in the middle section was well elevated in 18 orbits (75%).

In three orbits (13%) the posterior part of the graft was hanging 5 mm caudally. In six orbits (25%) the angle of the graft was graded as poor. The graft was at the wrong angle coronally in five and sagittally in four cases leading to an enlarged orbital volume in five (21%) orbits. At the last follow-up CT imaging showed that in one orbit the graft was still in an over-elevated position. All grafts were either moderately (79%) or mildly (21%) resorbed, but none had totally disappeared (Figures 25 A and B). On the other hand, new bone growth was observed in 75% of the cases.

Comparing with CT, MRI gave a more accurate view of the position of the soft tissue relative to bone. No muscle herniation was noted. In 15% of the orbits periorbital fat was seen protruding through the remaining bone defects. No maxillary sinus irritation was seen at the last visit. In the patient with the re-reconstructed orbital walls, CT and

MRI confirmed a good position and only moderate resorption of the bone.of the iliac grafts.

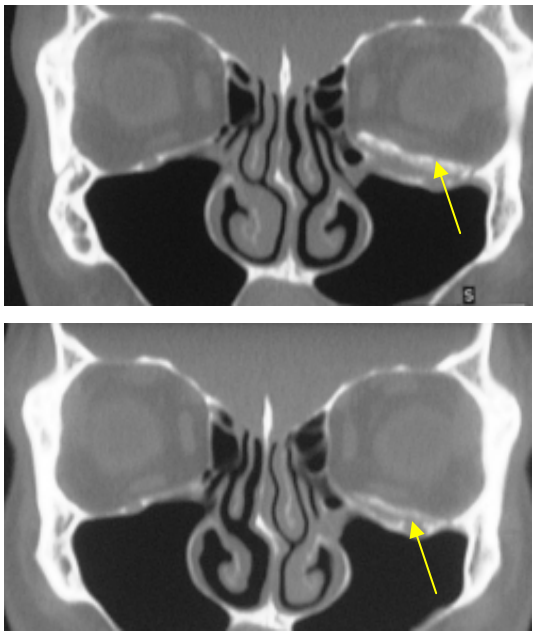

Figures 25 A and B.
Autogenous bone graft reconstruction (arrow) of the left orbital floor; A. 2 months after operation coronal CT shows resorption of the graft. B. 6 months after operation the graft has resorbed further. Note moderate ossification laterally in the area between the graft and the original orbital floor.

5.3. Finite element analysis (V)

Orbital displacement

Each simulated missile impact (blunt injury) caused the orbit to deform in a different way. Antero-lateral views from the FEM analysis are shown in Figures 26 A-E.

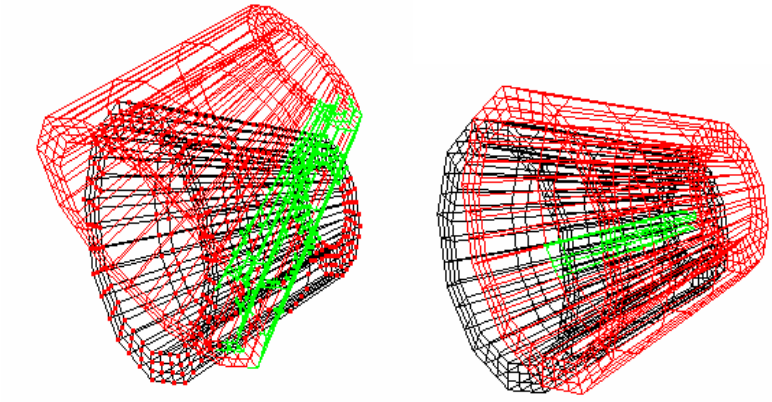

A. Missile impact from the front (MOR).
Maximum displacement = 117.8 mm

B. Missile impact from 45° upward (MU).
Maximum displacement = 91.3 mm

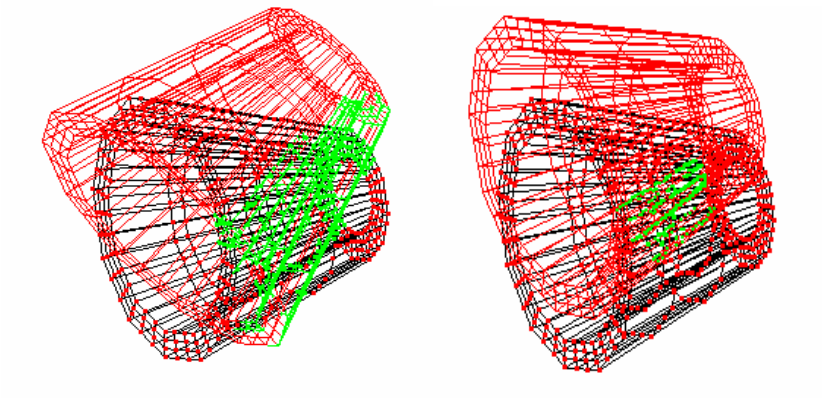

C. Missile impact from 45° downwards (MD).
Maximum displacement = 100.7 mm

D. Missile impact from 45° right (MR).
Maximum displacement = 75.6 mm

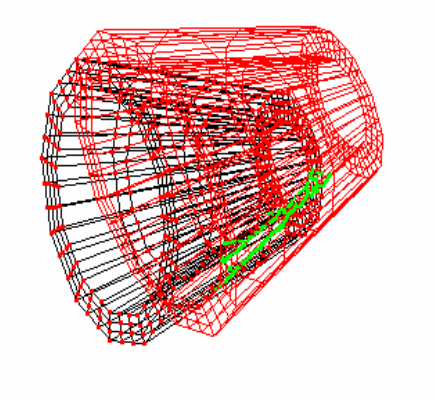

E. Missile impact from 45° left (ML).
Maximum displacement = 55.7 mm

Figures 26. **A, B, C, D, E.**
Antero-lateral view of the FEM in its non-deformed (black) and deformed (red) states during various simulations. Green indicates maximum deformation affecting the postero-medial part of the orbital floor. The display of the deformed state was magnified 10 times and the globe was omitted to make the distinction more evident.

The missile impact was simulated at right angles from the front to the orbital rim (MOR), 45^0 upwards (MU), 45^0 downward (MD), 45^0 right (MR) and 45^0 left (ML). The non-deformed state in each figure depicts the model with its structural elements in their unloaded condition. The deformed state is one in which the action of the missile displaced the structural elements, and the model has reached the state of static equilibrium. Displacement has been magnified in the figures to make orbital deformation more evident. When the missile was directed from the front or from 45^0

downwards, the orbit deformed in the anti-clockwise direction, and the lateral wall bent upwards and inwards, indicating orbital rotation. If the missile was directed from 45^0 right or from 45^0 left, the right and left sides of the orbit deformed turning anti-clockwise and clockwise respectively. If the missile was directed from 45^0 upwards, the lateral and medial walls were displaced in an outward direction, rather than being rotated, indicating less orbital rotation than from the impact coming from downwards and at right angles from the front.

Orbital stresses

Stress values ranged from 112.1 to 262.3 MPa for the maximum principal stress, from – 123.7 to – 552.1 MPa for the minimum principal stress, and from 111.3 to 343.3 MPa for the maximum shear stress (Table 8). In all cases the maximum stress occurred in the postero-medial part of the orbital floor (Figures 27 A and B.).

Table 8.
Maximum stress values predicted by the FEM analysis during simulated orbital injuries.

MAXIMUM STRESS (MPa)	Direction of the missile impact with a 30 m/s velocity			
	45° Upwards	**45° Downwards**	**45° Right**	**45° Left**
Maximum Principal	112.1	262.3	158.2	162.3
Minimum Principal	-226.8	-552.1	-123.7	-152.1
Maximum Shear	111.3	343.3	129.8	233.3

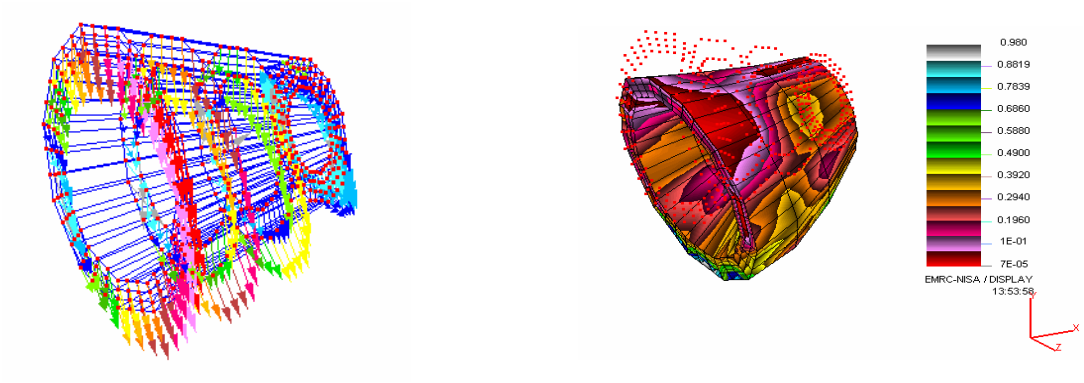

A. B.

Figure 27.
A. Deformation shown in the form of a vector display of maximum principal stress. The highest values (blue arrows) affected the postero-medial part of the orbital floor.
B. Maximum principal stress bands on the orbit when subjected to a blunt injury from a missile velocity 30 m/s, directed at right angles from the front to the orbital rim. Coloured numbers reflect stress magnitudes. To enhance the distribution patterns of principal stresses on the cortical surface of the orbit, the stresses were displayed at lower ranges of magnitude.

Orbital floor stresses

Special attention was given to the orbital floor stress analysis due to its importance in the treatment of orbital trauma. Stresses were quantified for loads (missile) coming at right angles from the front to the orbital rim (MOR), 45^0 upwards (MU), 45^0 downwards (MD), 45^0 (MR) and 45^0 (ML). In all cases, the impact coming from right and from left evoked the lowest stress magnitudes (Figures 28 A – D).

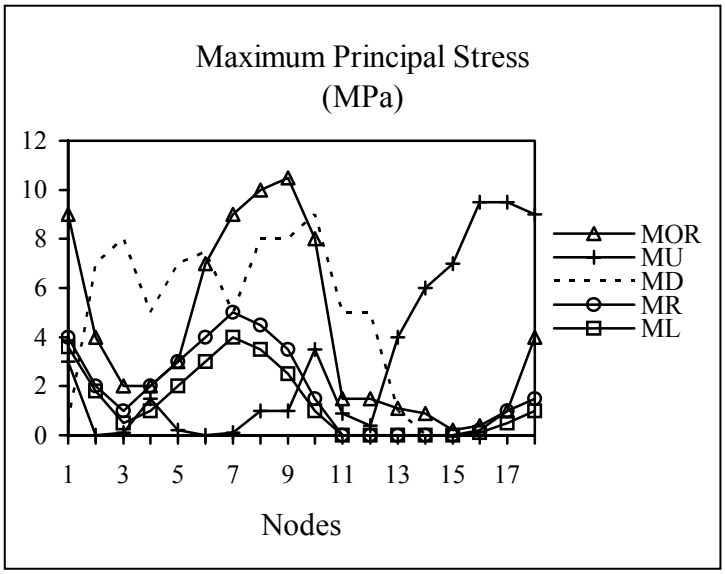

A.

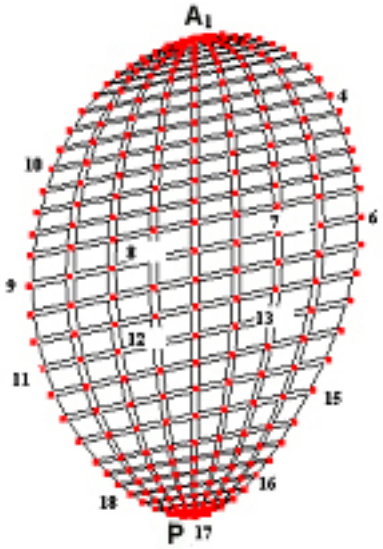

B.

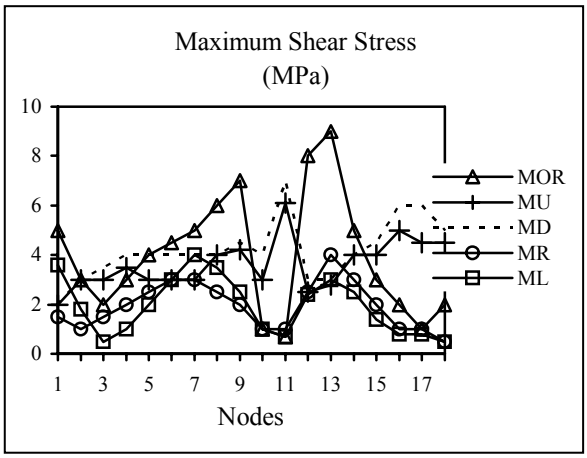

C.

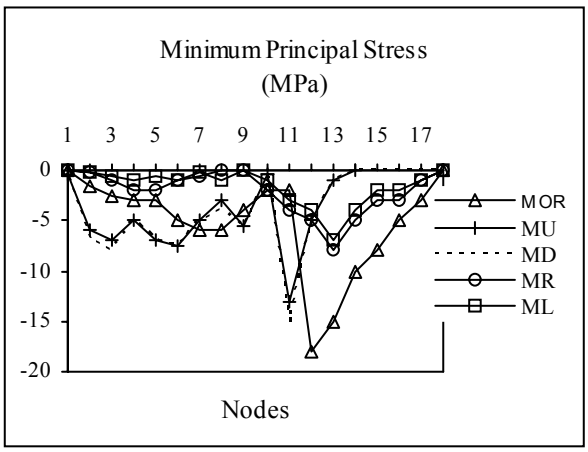

D.

Figure 28.
Principal (A and D) and maximum (C) shear stress magnitudes at the orbital floor during various simulations. Stress values were plotted at 18 nodes forming the cortical outline of the orbital floor (B.). Nodes 2 to 9 were located on the anterior (A) aspect of the orbital floor outline and nodes 11 to 18 on the posterior (P) side.

Maximum principal stress was higher at the posterior aspect of the orbital region than anteriorly during all simulations except the upwards impact, which resulted in higher magnitudes of stress at the anterior region of the floor. In all cases, the lowest values were found at the most lateral/medial sides. Minimum principal stresses had peaks of intensity at the anterior aspect of the orbital floor during upwards, downwards and at right angles from the front impacts. The magnitudes of maximum shear stress were approximately symmetrically distributed between the anterior and the posterior aspects

of the orbital floor region during all simulations except that in which the load was applied at right angles from the front to the orbital rim, which caused higher shear on the anterior orbital floor.

The average, maximum and total force magnitudes for 36 nodes forming the cortical outline of the postero-medial part of the orbital floor, during various simulations, are shown in Table 9. Although slightly dissimilar in total magnitude, the orbital forces were similar when the load was applied at right and left angulations. When the load was directed at the orbital rim at right angles from the front, in upwards or in downwards angulation, the postero-medial region experienced the highest average and total forces overall.

Table 9.
The average, maximum and total forces (Newton) are given for 36 nodes forming the cortical outline of the postero-medial part of the orbital floor.

Orbital Force (N)	Direction of the missile velocity 30 m/s				
	From the front at right angles	**45° Upwards**	**45° Downwards**	**45° Right**	**45° Left**
Average	8.4	8.2	7.9	6.3	6.4
Maximum	8.9	8.4	8.0	7.6	7.8
Total	199.3	187.0	182.1	175.0	176.0

6. DISCUSSION

Reconstruction of the orbital floor with bioresorbable materials is a controversial subject. No material has yet proven to be successful without any complications in clinical work. One of the main issues is the maintenance of the initial 3-dimensional shape of the implant. To achieve this, the implant needs to resist coiling and deformation and to be strong enough to tolerate the pressure exerted by the orbital content without being passively moulded. Another important issue is biocompatibility. The ideal material should have biological and physical properties that replicate those of the tissue it replaces. The material should be permanently accepted by the host, unless the implant material degrades completely within accetable time limits.

The material and biological properties of four different bioresorbable implants and autogenous iliac bone grafts were assessed in this study. Assessment of the implants involved a macroscopic evaluation, determination of strength and molecular weight and thermal and SEM analysis. Host response was assessed using TEM and immunohistochemistry. We chose tenascin, cellular fibronectin, α-actin-containing myofibroblast, type I collagen and type III collagen as biological markers for several reasons. Tenascin plays a role in the development of granulation tissue, in cell migration and in tissues undergoing active remodelling (Mackie *et al.* 1988, Luomanen and Virtanen 1993). In wounds, a marked transient increase has been detected in the expression of tenascin and cellular fibronectin (Luomanen and Virtanen 1991, 1993, Raghow 1994). Myofibroblasts play an important role in connective tissue capsule formation and maintenance, in particular capsular contraction (Welch *et al.* 1990). They generate the force that results in contraction of the capsule surrounding the implant (Welch *et al.* 1990). Collagen bundles also seem to be part of the tethering system that links the wound matrix to the surrounding tissues, enabling contractile forces to be transmitted across the wound or around the implant (Welch *et al.* 1990, Lossing and Hansson 1993).

Strength retention and reconstruction properties of polydioxanone and polylactide implants

PDS

Merten and Luhr (1994) reported that PDS looses 50% of its strength during the first postoperative month. We found that the PDS implant lost its shape completely during the first few postoperative weeks. Our results showed that the molecular weight of the

PDS decreased by over 50% during first month and by a further 50% during the second month, indicating a rapid loss of strength. This parallels other studies, in which the strength of the PDS plate was 50% of its original value four weeks after implantation and only 25% after five weeks (Hidding *et al.* 1991). Mäkelä and coworkers (2002) compared the breaking strength of SR PLLA, PDS and polyglyconate sutures of 0.3 – 0.5 mm in diameter. While SR PLLA retained its tensile strength up to 10 months, the PDS suture lost its tensile strength completely within five months. Highest percentage elongation of straight sutures (62%) was exhibited by PDS. For this reason PDS sutures have not been recommended for wound closure needing prolonged support such as bone.

Enophthalmos is generally detected in 30 – 70% of patients after blowout fracture (Greenwald *et al.* 1974, Bartkowski and Krzystkowa 1982, Kranau *et al.* 1991). In the present study only 13% had enophthalmos preoperatively. This is probably because preoperative examinations were performed on average only a few days after trauma when the swelling had not yet resolved. This is supported by the observation that at the end of the study almost half of the patients had enophthalmos or hypo-ophthalmos. Other research groups have reported similar high rates of enophthalmos in orbits reconstructed with PDS (Dietz *et al.* 2001, Baumann *et al.* 2002). These results seem to be slightly worse than in studies in which allogenic dura or nonresorbable implants have been used (Greenwald *et al.* 1994, Friesenecker *et al.* 1995).

Sixty years ago Pfeiffer (1943) noted that loss of bone support led to enophthalmos. However, loss of ligament support, fat atrophy and scar contracture may also lead to similar symptoms (Putterman 1991). We used CT and MRI imaging to try to establish the reasons for the high degree of enophthlmos after PDS reconstruction. While CT revealed new bone formation over the fracture area, the shape of the fractured floor and its craniocaudal height showed no marked change from the preoperative situation. On the other hand, MRI scans showed no fat herniation into the maxillary sinus. This suggests that the globe support during the healing period was inadequate and the volume of the orbit was not actually corrected. The fact that PDS degrades rapidly and loses much of its strength during the first few weeks is probable reasons for this. PDS is not able to withstand the pressure caused by orbital content. The scar that forms after implant resorption is too weak and thin to provide adequate support to the globe and to compensate for the enlarged orbital volume.

Although Merten and Luhr (1994) recommended PDS implants for reconstruction even large and anatomically demanding orbital defects, they reported that only morphologically intact implants had osteoconductive capabilities and that the resorbed PDS implants were replaced only by a tight scar tissue. Many studies suggest that PDS should only be used for minor orbital floor fractures (Iizuka *et al.* 1991, Baumann *et al.* 2002). Our study further supports this conclusion.

Polylactides

All resorbable SR PLDLA 96/4 and 85/15 copolymer implants coiled and fractured in our study. This significant degree of coiling was unexpected and has not previously been reported when plates are used for facial fracture treatment. Polylactide implants have been used for orbital floor reconstruction since 1972, when Cutright and Hunsuck (1972) published their study on their use in experimental fractures in rhesus monkeys. Since then there have been several studies on polylactide implants in orbital wall reconstruction (Rozema *et al.* 1990, de Roche *et al.* 2001) and in subcutaneous tissue (Cordewener *et al.* 1995) but none of them has reported any coiling. There have been no reports of coiling or deformation of SR strengthened plates in cases where the plates were symmetrically fixed with screws or pins (Suuronen 1993, Haers *et al.* 1998). However, in the orbital region such a symmetrical fixation of the plate both anteriorly and dorsally is not possible for anatomical reasons, which probably goes someway to explaining this difference.

The other main difference between the present and other studies on orbital implants is in the technique used to reinforce, i.e. strengthen, the plates. The material in our study was strengthened using the SR technique. Others have used the s.c. as-polymerized PLLA or PLDLA technique without strengthening (Rozema *et al.* 1990, Cordewener *et al.* 1996).

In the study by Rozema and coworkers (1990) PLLA sheets were used to reconstruct the orbital floors of goats. The authors reported that the orbital floors healed completely during the 78 weeks follow-up. At that time the plates were not yet fully disintegrated. Similar plates were later used in the reconstruction of orbital floor fractures in six patients (Cordewener *et al.* 1996). At the end of the follow-up time of between 3.5 and 6.5 years none of the patients reported any problems. MRI studies showed no abnormal tissue reactions or implant deformities in the orbital region. The authors concluded that PLLA orbital floor implants can be successfully used in the repair of human orbital

floor defects. The main drawback of PLLA is its very long degradation time, which is why it has not been recommended for orbital wall reconstruction (Bergsma *et al.* 1993, Andriano *et al.* 1994).

PLDLA stereocopolymers have been developed to shorten the degradation time of PLA-based implants. The degree of crystallinity and strength retention can be modulated by changing the optic isomer (L/DL) ratio. *In vitro* the degradation time of the PLDLA has been shown to be shorter than that of pure PLLA, yet its strength properties are comparable to those of pure PLLA (Andriano *et al.* 1994). On the other hand, some major unfavourable changes related to the mechanical and physical properties of PLDLA stereocopolymers, such as rapid loss of strength, have been reported to occur during the first few weeks after *in vivo* implantation (Cordewener *et al.* 1995).

The present experimental study examined the suitability of resorbable SR PLDLA 96/4 and 85/15 copolymer implants for orbital floor reconstruction. Unfortunately, the mechanical and physical properties of these plates were poor. When the orbital floor was reconstructed with the SR PLDLA 96/4 implant, no differences were seen in healing between the reconstructed and control orbital floors. As with PDS, copolymers loose their strength much faster than PLLA homopolymer. The shear strength of SR PLDLA 96/4 polymer decreases by about 30% from its initial value in 16 weeks. Thereafter the shear strength could not even be measured because of the fragility and particulation of the implant material. The tensile strength of SR PLDLA 85/15 was not measurable after four weeks. This parallels the studies by Cordewener and coworkers (1995). Thus, these materials cannot be safely used for orbital floor reconstruction, either. The decrease in shear strength and subsequent resorption occur too early and, hence, the plate cannot tolerate the pressure caused by the orbital content.

Clinically, the orbits showed better ossification than was expected based on radiological imaging. This was due to the fact that the bone formed was very thin and not always visible in radiographs. Therefore, the problem seems not to be that the orbital floor does not ossify, as this seems to happen. However, bone heals too caudally and results in a further and harmful increase in orbital volume.

To avoid these problems, and in particular to avoid coiling, a new SR (P(L/DL)LA 96/70 orbital-floor implant was designed composed of a frame of 70/30 L/DL-lactide copolymer and 96/4 L/D-lactide copolymer mesh sheet.

The SR P(L/D)LA 96/4 mesh of the implant seems to degrade more slowly than the SR P(L/DL)LA 70/30 frame. During the first three months the molecular weights decreased only by 25 %, both materials having the same molecular weight at that time. But after seven months follow-up the molecular weights decreased to 50% (SR P(L/D)LA 96/4) and to 20% (SR P(L/DL)LA 70/30). The change in crystallinity of both materials was only minor. This was expected according to the literature on SR strengthened polylactide copolymers (Pohjonen 1995) and the results are better than of those for as-polymerized L/D polylactides (Cordewener *et al.* 1995). On the other hand, in scanning electron microscopy, both SR-P(L/DL)LA materials degraded significantly during the 7-month follow-up *in vivo*. The surface of the plate showed significant changes and became partially detached from the porous core during that time. Cracking was observed at the outer curve of the filament loop. The findings parallel other published reports (Pohjonen 1995). During the follow-up there were no signs of deformation or coiling. The mechanical and physical properties seem to be suitable for orbital floor reconstruction, but further studies are needed to validate these preliminary findings.

Biocompatibility of polydioxanone and polylactide implants

Many clinical and experimental studies have concluded that biodegradable PDS implants are well tolerated in the orbital region (Merten and Luhr 1994), although contradictory publications exist. There are numerous reports of adverse foreign body reactions related to PDS (de Roche *et al.* 1998, Baumann *et al.* 2002). Capsules surrounding breast implants removed due to complications seem to be composed of two zones, an inner cell-rich zone and an outer dense connective tissue zone (Lossing and Hansson 1993). This organization of peri-implant tissues into an inner zone and a dense outer fibrous zone was detected around PDS implants in our study, too. The inner cell-rich zone resembled granulation tissue and was of restricted localization. Degrading implant crystals generate a foreign body type reaction leading to capsule formation (de Roche *et al.* 1998). The mechanism controlling the formation of the capsule and the reactive and adaptive changes associated with it are not known. It has been proposed that the local enrichment of growth factors, which are beneficial for acute wound healing, in the chronically irritated tissue around resorbing implants support adverse tissue reactions (Lossing and Hansson 1993).

Using MRI imaging we demonstrated a foreign body reaction and fluid accumulation in more than half of the patients with a PDS orbital wall implant. Our experimental studies showed an increase in inflammatory cells in the capsule around the PDS implant, indicating a foreign body reaction. These results confirm those reported by de Roche and coworkers (1998) and Bar and coworkers (1992).

We were able to demonstrate a perpetuated expression of the extracellular matrix proteins tenascin, cellular fibronectin and also of α-actin (active myofibroblasts) in the capsule around PDS. The basic reasons for this are obscure. The simultaneous reactivity for tenascin, collagen type III and active myofibroblasts is a very important issue. This finding of prolonged persistance of granulation tissue is a sign of an active and ongoing process around the biodegradable PDS implant and should be considered when the clinical use of this material is contemplated for the orbital reconstruction.

An inner cell-rich zone and a dense outer zone of the capsule were also detected around all polylactide copolymer implants. The inner zone appeared in the very early phase. Cells were attached to the implant surface and were continuously in contact with the implant material. Only a mild foreign body reaction was detected. Expression of all the ECM proteins studied was demonstrated in the connective capsule around polylactide implants. The finding of two different zones coincided well with these tissue markers. The cell-rich zone corresponded with the expression of tenascin and collagen type III, whereas the outer connective tissue zone was characterized by the expression of collagen type I and α-actin. The presence of tenascin, cellular fibronectin and collagen type III in the zone immediately surrounding implants has also been noted in other studies (Lindholm *et al.* 1996, Shannon *et al.* 1997).

During wound healing tenascin is expressed in the granulation tissue, where it declines just before the wound heals completely (Luomanen and Virtanen 1993). Similar results were obtained in the present study. Wound contraction and contraction of the capsule around the implant have been shown to be attributed to the activity of myofibroblasts, which are rich in α-actin bundles (Lossing and Hanson 1993, Shannon *et al.* 1997). Some but not all fibroblast-like cells in dense connective tissue zones synthesize α-actin (Welch *et al.* 1990). In the present study, considerable α-actin reactivity (active myofibroblasts) was found in the outer zone of the PLDLA capsule. They formed a tight belt around the implant and the inner cell rich zone in contact with it throughout the study period.

Several experimental and clinical studies have been conducted on the biocompatibility of SR polylactides. Except for a low-grade foreign body reaction they have proved to be well tolerated (Vainionpää *et al.* 1989, Suuronen 1993, Gogolewsky *et al.* 1993). In the present study no adverse reactions to polylactide copolymers were noted, except for fluid accumulation in the implant capsule. The fluid reflects a typical, non-specific, foreign body reaction without signs of infection, supporting the results of earlier studies (Böstman *et al.* 1992, Thaller *et al.* 1995). However, the prolonged appearance of granulation tissue with increased ECM protein reactivity reflects a prolonged, active process around the biodegradable implant and should be taken into consideration in the clinical use of polylactide materials.

Reconstruction properties of autogenous iliac bone grafts

Autogenous bone grafting has been the gold standard providing framework for the facial skeleton and orbital walls. Bone grafting is the method of choice for correction of posttraumatic globe malposition (Roncevic and Malinger 1981, Hemprich and Breier 1993, Siddique and Mathog 2002).

Many different sources of autogenous bone such as calvarium, mandibular and maxillary bone, ribs, and iliac crest are available (Lee *et al.* 1998, Mintz *et al.* 1998, Dempf *et al.* 2001, Siddique and Mathog 2002, Ellis and Tan 2003). In the study by Ellis and Tan (2003) calvarium bone was compared with titanium mesh in 38 patients for internal orbital wall reconstruction. They concluded that both titanium mesh and calvarium bone can be successfully used for reconstruction of isolated blowout fractures. However, there was significant variance in the cross-sectional area of the anterior region of the orbit. Furthermore, because of its brittleness, calvarium bone could not be contoured to adapt to the complex structure internal orbit. Dempf and coworkers (2001) used calvarial and iliac crest grafts in repairing osseous orbital defects. Of 42 patients 34 were followed up for at least four months. They concluded that with autogenous bone transplants, good aesthetic and functional results can be achieved, and that autogenous grafts can be broadly recommended. Calvarium split grafts were particularly suitable for this purpose. Both Bartkowski and Krzystkowa (1982) and de Visscher and van der Wal (1988) used iliac crest grafts for orbital floor and medial wall reconstruction. Both study groups concluded that autogenous corticocancellous bone, like iliac crest, is extremely well tolerated and is suitable for orbital wall reconstruction. On the other hand, an iliac crest graft is said to be bulky

unless trimmed and it may resorb unpredictably (Roncevic and Malinger 1981). Resorption of iliac bone grafts used for orbital wall reconstruction has been clearly documented (Sullivan *et al.* 1993, Iatrou *et al.* 2001, Siddique and Mathog 2002).

Basically there are two forms of free autogenous bone graft: cortical and cancellous (Burchardt 1983). They differ in their mechanical properties. The mechanical strengths of cancellous and cortical grafts correlate with the respective repair process: cancellous grafts tend to strengthen first, whereas cortical grafts become weaker (Burchardt 1983). In the present study corticocancellous bone grafts were used. The results of the resorption were consistent with earlier studies. In 80% of the orbits major resorption was observed. However, the height of the graft was poor in only two (11%) out of those orbits. On the other hand, when only mild resorption of the graft was observed, the height of the graft was poor in 20% of those orbits.

At the end of the follow-up the outcome of the bony reconstruction was graded poor in 25% of orbits. In those orbits in which the orbital volume had increased, the angulation of the graft was improper. At the same time new bone growth was observed in 75% of orbits. This suggests that, on the one hand, at least to some extent, resorption and remodelling of the corticocancellous graft is anatomically beneficial and on the other hand that exact primary 3-dimensional correction of the fractured walls and correct angulation of the graft are very important for an adequate anatomic outcome. It is notworthy that intraoperatively the iliac graft was moldable and after trimming was easily adapted to the shape and form of the internal orbital wall.

The principal mechanism of posttraumatic enophthalmos and hypo-ophthalmos is enlargement of the volume of the orbit (Pfeiffer 1943, Manson *et al.* 1986). In the present study using iliac bone graft reconstruction only one patient had enophthalmos and five (21%) had hypo-ophthalmos after the follow-up. These results are satisfactory and well parallel to other studies (Greenwald *et al.* 1974, Bartkowski and Krzystkowa 1982, de Visscher and van der Wal 1988, Friesenecker *et al.* 1995). In the five cases, in which enlarged volume of the orbit was observed, the bone graft was placed too caudally in the posterior floor area. This coincides well with the study by Ellis and Tan (2003).

In the present study group, one patient needed a reoperation because of inadequate primary graft placement. In spite of the good radiological results after rereconstruction, his final clinical outcome was unsatisfactory. Meticulous analysis of both MRI and CT

images did not reveal the exact reason for the false position of the globe. This experience emphasizes the significance of succesful primary correction.

The study by Iatrou and coworkers (2001) reported that hypo-ophthalmos remains in the most severe cases despite of moderately good bone graft reconstruction. They suggested that the reason for this is the unfavourable bone resorption. Dempf and coworkers (2001) reported 30% hypo-ophthalmos rate after orbital wall reconstruction, although the reconstruction was rated anatomically poor in only 2% of cases. They used calvarial and iliac crest grafts to repair osseous orbital defects. In the present study moderate or major bone resorption was observed in 80% of orbits. Clinically these patients had no enophthalmos. This parallels well above mentioned studies and is indicative of the favourable mechanical properties of iliac bone grafts.

Overcorrection of the fracture area is recommended by Iatrou and coworkers (2001). In the present study only one patient had clinically demonstrated hyperophthalmos. He was the only one, whose graft was in an overcorrected position. Although the number of patients is small in this study, it seems reasonable to assume that fresh blowout fractures do not need to be overcorrected with an iliac bone graft, but the graft should be positioned accurately.

Donor site disadvantages of autogenous iliac bone grafts

The disadvantages of autogenous iliac bone grafts include donor site nerve and blood vessel injuries, acute and chronic pain, gait problems, and cosmetic disturbances. Although multiple sites can be used harvest autogenous grafts, the anterior iliac crest remains the most popular donor site (St John *et al.* 2003). Despite the large volume of autologous iliac crest grafts used, donor site morbidity seems to be low. A study by Banwart and coworkers (1995) revealed that none of the 261 patients studied had a severe perioperative complication and none of the 225 patients in a long-term follow-up had a severe late complication. The authors concluded that severe complications from iliac crest bone graft harvesting can be avoided by proper surgical methods and that major complications affecting function are uncommon, although minor complications are relatively common. Ahlmann and coworkers (2002) reported similar results in their study of 66 anterior iliac sites. Major complications were seen in 8% and minor ones in 15%. In our study the most common complication was a visible skin scar. Five patients (20%) ended up having a visible scar in this area. The incision in the iliac crest area

should be carefully planned, especially in female patients. Although the rate seems to be low, donor site complications should not be ignored.

Diplopia and orbital wall reconstruction

Patients who experience true diplopia naturally are quite troubled by this symptom and nearly always present this as their chief complaint. Basically, diplopia may be monocular or binocular. The two most common hypotheses for binocular double vision and impaired eye movement are contusion injury to the extraocular muscles or soft tissues and incarceration of these structures to the fracture line (Converse and Smith 1967, Putterman *et al.* 1974). Our patients had double vision in most cases in upward gaze, and movement limitation upwards. This can be explained by these two mechanisms.

MR imaging has been reported to be sensitive for orbital fat, orbital muscles and haematoma (Manfre *et al.* 1993, Zhan *et al.* 1995). In the present study all these structures were clearly visualized by MRI. On the intact orbital floor, the orbital fat faced the straight bony floor. Therefore, the flat inferior rectus muscle was well visualized leaning on the orbital floor. On the fractured side the orbital fat protruded as a round mass into the maxillary sinus. The inferior muscle was considerably rounded compared to flat-shaped muscle at the uninjured site, giving an impression of being oedematous. MR imaging demonstrated the presence of a thin fat layer between the fractured bone and the inferior muscle. When preoperative MRI and CT taken from the same fracture were compared, no trap door fracture or muscle incarceration was documented and neither was seen in postoperative CT or MRI scans. In addition, postoperative MRI showed that infraorbital tissue was well repositioned on top of the bone graft.

Diplopia was seen more often immediately postoperatively (84%) than preoperatively (75%). This is probably due to iatrogenic surgical injury, e.g. slight haemorrhage, contusion, postoperative oedema and scar formation. MRI revealed that the inferior rectus muscle was still oedematic in 44% of the patients at the last visit, which, however did not correlate with diplopia. No correlation could be established between the position of the bone graft and diplopia in this study. Operation delay did not affect the occurrence of postoperative diplopia, either. This parallels other studies, suggesting that diplopia is multicausative rather than the result of an increase in orbital volume, contusion or incarceration only. Early surgery is not necessary for treatment of diplopia

if no evidence of entrapment is detected (Catone *et al.* 1988, Putterman 1991). The present findings agree well with this conclusion.

A forced duction test is used if incarceration on intraorbital soft tissue or ophthalmoplegia is suspected. Kupersmith and Fazzone (2004) evaluated three portable methods for documenting ocular muscle limitation that might be used at multiple sites in a clinical trial. They concluded that the intra-examiner repeatability of measurements was high but considerably less than the intra-examiner repeatability in all three test methods. Although the forced duction test was neither included in the study protocol nor studied, it was found beneficial in cases where ophthalmoplegia was suspected.

Finite element modelling

Although treatment of orbital fractures has a moderate success rate, the long-term clinical significance of orbital deformation through implant treatment is still unknown. The possibility that traumatic orbital deformation and the resulting stresses may lead to implant failure cannot be excluded. FE modelling provides insights into the understanding of this multifaceted phenomenon, which has relevance to clinical practise.

A review of the literature showed that several three-dimensional finite element models of the eye and/or orbit have been created (Kobayashi *et al.* 1971, Power 2001). Generally speaking, the reliability of their predictions for modelling has been severely compromised by oversimplification of the orbital geometry, material properties and/or boundary conditions. The accuracy of a finite element model (FEM) in predicting strains directly depends on the accuracy of these effectors in the environment.

The anterior aspect of the orbital floor was affected most at lower magnitudes of principal stresses than the posterior aspect. This might be explained by the cushioning effect of the eyeball and underlying fatty tissues, which provides an ideal stress-breaking mechanism to minimize orbital deformation. This highlights the importance of restoring the fatty tissue during orbital floor reconstruction following an orbital blowout fracture. Our investigation confirms reports by Waterhouse and coworkers (1999), that the buckling mechanism produces fractures in the posterior and postero-medial aspects of the orbital floor and that, in contrast to the result expected from the hydraulic mechanism, medial wall involvement is infrequent. According to the buckling theory, direct trauma to the orbit may cause transient deformation of the infraorbital rim. This is transmitted to the thinner orbital floor causing its disruption without a fracture of the

rim. The hydraulic theory, in contrast, proposes that the hydraulic pressure from the globe is transmitted to the walls of the orbit, resulting in fracture of the orbital floor.

The qualified usefulness of the finite element model developed in this study lies in the facts that a) it modelled bone as an orthotropic material, b) the model was loaded with experimentally obtained muscular forces, c) it was mathematically validated, and sensitivity analysis was used throughout to enhance the equivalency of the model to a real human orbit. It is this detailed and comprehensive approach that gives the model a reliability that has so far been missing in the finite element models reported in the literature. However, finite element modelling and its applications in the management of orbital fractures are still in their infancy. New research is going on in this field and we hope to come up with better materials or methods to treat the challenging problem of orbital wall fracture.

7. CONCLUSIONS

The following conclusions can be drawn from the results obtained in the present studies:

1. Mechanically, PDS sheets are poor as they loose their shape and integrity completely within a few weeks. The molecular weight of PDS falls rapidly already during the first month. Degradation of PDS is seen as detaching particles from the plate surface. After two months PDS folio degrades into hard, sharp pieces. Peri-implant reactions such as thick scar tissue formations and fibrotic sinuses appear. A PDS implant does not restore the orbital volume, nor does it provide adequate support for orbital contents. Posttraumatic enophthalmos or hypo-ophthalmos can not be prevented.

2. With the exception of SR PLDLA 96/70 mesh sheet – frame composites, the mechanical properties of polylactide implants are not suitable for orbital wall reconstruction. Both SR PLDLA 85/15 and 96/4 implants lose their strength too fast. Macroscopical examination shows that both these implants are severely deformed after a few weeks. On the other hand, the molecular weights of SR P(L/D)LA 96/4 and SR P(L/DL)LA 70/30 decrease slowly and, accordingly, an SR PLDLA 96/70 composite implant maintains its shape adequately. The mesh sheet - frame structure seems to be mechanically adequate for orbital wall reconstruction.

3. All the cell markers (Tn, cFn, α-actin and type I and type III collagen) studied here are expressed widely in the connective tissue capsule forming around PDS and polylactide materials. Their expression continues throughout the whole observation period, indicating an ongoing, long-term host response. There seems to be no differences between SR PLDLA, SR PLDLA 96/70 composite and PDS implant materials in relation to the immunohistochemical findings studied here, indicating that the response is directed against the bulky implant *per se*, rather than being dependent on its exact physicochemical properties. The cell-rich interface zone, together with the increased reactivity of the markers, indicates an active process around the biodegradable implants

and should be taken into account when the clinical use of these materials is being considered. It seems that PDS gives rise to inflammatory reactions. Although these reactions are usually mild, often even clinically unnoticed, it is obvious that the use of this material carries with it the risk of severe inflammatory complications.This may be an issue with all biodegradable materials.

4. Reconstruction of the orbital wall with an autologous iliac bone graft is reliable. It restores the volume and the shape of the orbit well. The resorption rate is high, but most of it is beneficial remodelization. The graft is rigid enough to support the orbital contents and facilitates new bone growth across the orbital wall defect. Autogenous bone grafts have obvious advantages over the resorbable materials studied here.

5. Our study group constructed and reports a finite element model that represents the human orbit housing the eyeball and its associated structures. The stresses and forces required to produce an orbital fracture are for the first time numerically modelled. However, more work must be done to study the effects of changing the geometrical relationships, material properties and boundary conditions on stress/strain readings and their role in successful fracture treatment.

8. SUMMARY

Autogenous bone grafts provide the "gold standard" for orbital reconstructions. However, they are rather complex to use in routine clinical praxis. This problem could be overcome by the use of alloplastic material, which is readily available and easy to handle. However, alloplastic materials have been used with caution, because they can provoke unpredictable foreign body reactions. It is this background that led us to investigate the clinical performance and biocompatibility of these materials to be able to create evidence and recommendations for their use in the reconstruction of orbital wall fractures.

Three sets of experiments were undertaken. These were experimental, clinical and finite element analysis studies. In the experimental studies we used four different implant models in 10 rabbits, 18 sheep and 24 rats to examine the biocompatibility of three different self-reinforced polylactide stereocopolymers (SR PLDLA 96/4, SR PLDLA 85/15, SR PLDLA 96/70 composite) and polydioxanone (PDS®) implants. The study protocol included CT imaging, immunohistochemistry and electron microscopy. The clinical studies included two different models using a bone graft and a PDS® plate as implant material. In the first clinical study 24 consecutive internal orbital wall fractures were reconstructed using autogenous iliac crest bone grafts. In the second clinical study, 16 consecutive fractures were repaired using PDS® sheets. These study protocols consisted of clinical examinations and CT and MRI imaging. A finite element model (FEM) was constructed of the human orbit, including the eye, fatty tissues and extra-ocular muscles. The orbit was subjected to a blunt impact from a 0.5 kg missile striking the orbit at 30 m/s at different angles. The finite element model was then used to predict principal and shear stresses / strains at each node position.

In the experimental studies, all SR PLDLA and PDS® implants, except the SR PLDLA 96/70 composite implants, became severely deformed during the follow-up. After two months the PDS folio had degraded into hard, sharp pieces and the SR PLDLA implants had broken after a few weeks. The strength of SR PLDLA implants decreased rapidly and after a few months could not be measured. In contrast, the SR PLDLA 96/70 composite implants maintained their shape and strength throughout the whole observation period of seven months. All the implants were enveloped by a connective tissue capsule, consisting mainly of fibroblast-like cells. A low-grade chronic inflammation was observed. There was an intense reactivity for Tn, cFn and smooth muscle α-actin.

In the clinical studies, when PDS implants were used to reconstruct the orbital wall fracture, MRI revealed adverse peri-implant reactions in 10 cases (63%). No such lesions, i.e. foreign body reactions, were detected when autogenous bone grafts were used. CT imaging showed that there were no differences in the size or shape of the defects pre- and postoperatively when PDS implants were used. This agreed with the findings of the experimental studies. All free bone grafts were partially resorbed, but new bone growth was observed in 75% of the orbits and the volume of the orbit was restored. After PDS reconstruction of internal orbital wall fracture about 40% of the patients had enophthalmos. Following bone graft reconstruction, only one patient (4%) had enophthalmos.

The finite element analysis study demonstrated two types of orbital deformation: a) horizontal distortion and b) rotational distortion. Stress values ranged from 112.1 to 262.3 MPa for maximum principal stress, from –123.7 to –552.1 MPa for minimum principal stress, and from 111.3 to 343.3 MPa for maximum shear stress.

In short, reconstruction of the orbital walls was most reliable using autogenous iliac bone graft. It restored the volume and the shape of the orbit well. Autogenous bone grafts have obvious advantages over alloplastic resorbable materials. Of the resorbable implants studied here, only the mesh sheet and frame structure of the SR PLDLA 96/70 proved to be mechanically adequate for orbital wall reconstruction. There were no differences between polylactide implant materials and PDS implants in terms of immunohistochemical findings. The simultaneous increase in the reactivity of cell markers is an important issue related to the bioresorbable materials studied here, but this may also be the case with all biodegradable materials. The finite element model constructed is the first one reported that represents the human orbit housing the eyeball and its associated structures. In this study, the stresses and forces required to produce an orbital fracture were measured with reasonable reliability for the first time.

9.ACKNOWLEDGEMENTS

The present study was carried out at the Departments of Oral and Maxillofacial Surgery, Institute of Dentistry and Helsinki University Central Hospital and at the Institute of Clinical Medicine, Department of Maxillofacial Surgery, at the Department of Clinical Veterinary Sciences, at the Institute of Biomedicine and at the Department of Anatomy, Helsinki University and at the Institute of Biomaterials, Tampere University of Technology, during the years 1993 - 2005.

I wish to express my deepest gratitude to my highly respected teacher, Professor Christian Lindqvist, MD, DDS, PhD, Head and Surgeon-in-Chief of the Department of Oral and Maxillofacial Surgery, University of Helsinki. He patiently gave me his time, encouragement, support and guidance throughout this work. He was the supervisor of my thesis and provided me the excellent research facilities for this study.

I express my warmest gratitude to Professor Yrjö T. Konttinen, MD, PhD, the Department of Medicine, Helsinki University Hospital and Professor Ismo Virtanen, MD, PhD, the Institute of Biomedicine/Anatomy, Helsinki University the supervisors of this thesis, for their enthusiastic, broad-minded and inspiring attitude to research and the excellent research facilities they provided for me.

I am grateful to Professor Riitta Suuronen, MD, DDS, PhD, Professor in Medical Biomaterials and Head of REGEA - Institute for Regenerative Medicine, for suggesting the topic of the study to me and her encouraging support and experienced advice on several aspects of this research. I want to thank her for her endless patience and understanding which helped me through the hard times.

My special thanks are due to my colleagues, Professor Anna-Lisa Söderholm MD, DDS, PhD and Docent Pekka Laine, DDS, PhD, for their excellent and long standing support and experienced advice for designing and carrying out this research.

I am highly thankful to Docent Bertel Kommonen, VMD, PhD, Institute of Veterinary Medicine, University of Helsinki for his expert guidance, advice and great help in the experimental work.

My warm thanks are due to my excellent co-workers Professor Jukka Meurman, MD, DDS, PhD, Institute of Dentistry, Helsinki University Central Hospital, Professor Minna Kellomäki, Dr Tech, MSc (Eng.), Laboratory of Biomaterials, Tampere University of Technology, Dr Tarja Kylmä VMD, PhD, Institute of Veterinary Medicine, University of Helsinki, Docent Dorrit Hallikainen, MD, PhD, Docent Oili

Salonen, MD, PhD and Dr Pertti Paukku, MD, Department of Radiology, Helsinki University Central Hospital, Dr Pasi Ruuttila, MD and Dr Lauri Lindroos, MD, Institute of Biomedicine, Helsinki University and Dr Jehad Al-Sukhun, BDS, MSc, PhD, Department of Oral and Maxillofacial Surgery, Helsinki University Central Hospital, for efficient co-operation in the realization of this work.

I am greatly thankful to my colleagues Dr Karri Mesimäki, MD, DDS, Dr Antero Salo, MD, DDS, PhD, Dr Hanna Thoren, MD, DDS, PhD and Dr Jyrki Törnwall MD, DDS, PhD, Department of Oral and Maxillofacial Surgery, Helsinki University Central Hospital for their excellent support and their participation in the surgical part of this research.

Appointed by the Faculty of Medicine, University of Helsinki, Docent Matti Lamberg, MD, DDS, PhD and Professor Kyösti Oikarinen DDS, PhD read the manuscript. I greatly appreciate their competent advice and constructive criticism.

I wish to express my warm thanks to Ms Helene Victorzon and Ms Riitta Multala for their skillful assistance in all aspects of the administrative part of this research and for their enthusiastic support during this study.

My best thanks are due to Ms Paula Hasenson, for making specimens for microscopical studies and due to Mr Reijo Karppinen and Mr Hannu Kamppinen for skillful technical assistance.

I am thankful for the staff of Surgical hospital for the great support and for the opportunity to carry out this study.

My thanks are due to the Finnish PhD Graduate School in Biomaterials and Tissue Engineering of the Ministry of Education for their excellent support.

I wish to express my warmest thanks to my lovely family, my beloved wife Ulla, for her generous and devoted support throughout this long standing work and to my four children, Ilari, Riikka, Sirke and Karri for their continuous understanding of my absence. Without their support and love this study would not have been possible to carry out.

This project was supported by grants from the Finnish Medical Faculty, from the Finnish Dental Society Apollonia and from the special governmental subsidiary for health science research of the Helsinki University Hospital.

Helsinki 14.9.2005

10. REFERENCES

Ahlmann E, Patzakis M, Roidis N, Shepherd L, Holtom P. Comparison of anterior and posterior iliac crest bone grafts in terms of harvest-site morbidity and functional outcomes. J Bone Joint Surg Am. 84: 716-720. 2002.

Ahmad F, Kirkpatrick WN, Lyne J, Urdang M, Garey LJ, Waterhouse N. Strain gauge biomechanical evaluation of forces in orbital floor fractures. Br J Plast Surg 56:3-9. 2003.

Ahn DK, Sims CD, Randolph MA, O'Connor D, Butler PE, Amarante MT, Yaremchuk MJ. Craniofacial skeletal fixation using biodegradable plates and cyanoacrylate glue. Plast Reconstr Surg 99:1508-1515. 1997.

Aitasalo K, Kinnunen I, Palmgren J, Varpula M. Repair of orbital floor fractures with bioactive glass implants. J Oral Maxillofac Surg 59:1390-1395. 2001.

Al-Sukhun J. Modelling of Mandibular functional deformation. PhD thesis, University of London, London, UK. 2003.

Andriano KP, Pohjonen T, Törmälä P, Processing and characterisation of absorbable polylactide polymers for use in surgical implants. J Appl Biomat 5: 133-140. 1994.

Antonyshyn O, Gruss JS, Galbraith DJ, Hurwitz JJ. Complex orbital fractures: a critical analysis of immediate bone graft reconstruction. Ann Plast Surg 22: 220-233. 1989.

Aronowitz JA, Freeman BS, Spira M. Long-term stability of teflon orbital implants. Plast Reconstr Surg 78: 166-173. 1986.

Asplund O. Capsular contracture in silicone gel and saline-filled breast implants after reconstruction. Plast Reconstr Surg 73: 270-275. 1984.

Bagambisa FB, Kappert HF, Schilli W. Cellular and molecular biological events at the implant interface. J Craniomaxillofac Surg 22: 12-17. 1994.

Bahr W, Stricker A, Gutwald R, Wellens E. Biodegradable osteosynthesis material for stabilization of midface fractures: experimental investigation in sheep. J Craniomaxillofac Surg 27: 51-57. 1999.

Balza E, Siri A, Ponassi M, Caocci F, Linnala A, Virtanen I, Zardi L. Production and characterization of monoclonal antibodies specific for different epitopes of human tenascin. FEBS Lett 332 :39-43. 1993.

Banwart JC, Asher MA, Hassanein RS. Iliac crest bone graft harvest donor site morbidity. A statistical evaluation. Spine. 20: 1055-1060. 1995.

Bar BW, Tausch W, Buntrock P. Ligament repair with PDS (polydioxanone) in chronic insufficiency of the fibular ligament of the upper ankle joint: experimental and clinical experiences. Aktuelle Traumatol 22: 229-235.1992.

Bartkowski SB, Krzystkowa KM. Blow-out fracture of the orbit. Diagnostic and therapeutic considerations, and results in 90 patients treated. J Maxillofacial Surg 10: 155-164. 1982.

Baumann A, Burggasser G, Gauss N, Ewers R. Orbital floor reconstruction with an alloplastic resorbable polydioxanone sheet. Int J Oral Maxillofac Surg 31:367-373. 2002.

Bergsma EJ, Rozema FR, Bos RRM. Foreign body reactions to resorbable poly(L-lactide) bone plates and screws used for the fixation of unstable zygomatic fractures. J Oral Maxillofac Surg. 51: 666-670. 1993.

Bonutti PM, Cremens MJ, Miller BG. Formation of structural grafts from cancellous bone fragments. Am J Orthop 27: 499-502. 1998.

Breme J, Steinhäuser E, Paulus G: Commercially pure titanium Steinhäuser plate screw system for maxillofacial surgery. Biomaterials 9: 310-313. 1988.

Burchardt H. The biology of bone graft repair. Clin Orthop 174: 28-42. 1983.

Burkhardt BR. Capsular contracture: hard breasts, soft data. Clin Plast Surg 15: 521-532. 1988.

Burm JS, Chung CH, Oh SJ. Pure orbital blowout fracture: new concepts and importance of medial orbital blowout fracture. Plast Reconstr Surg 103:1839-49. 1999.

Böstman OM, Päivarinta U, Partio E, Manninen M, Vasenius J, Majola A, Rokkanen P. The tissue-implant interface during degradation of absorbable polyglycolide fracture fixation screws in the rabbit femur. Clin Orthop Relat Res 285:263-272. 1992.

Cantaloube D, Rives JM, Bauby F, Andreani JF, Dumas B. Use of a cup-shaped implant of polydioxanone in orbital-malar fractures. Rev Stomatol Chir Maxillofac 90: 48-51. 1989.

Caplan AI. The mesengenic process: Bone repair and regeneration. Clin Plast Surg. 21: 429-435. 1994.

Cashman S, Simpson CB, McGuff HS. Soft tissue response of the rabbit larynx to Gore-Tex implants. Ann Otol Rhinol Laryngol 111: 977-82. 2002.

Catone GA, Morrissette MP, Carlson ER. A retrospective study of untreated orbital blow-out fractures. J Oral Maxillofac Surg 46: 1033-1038. 1988.

Cheung D, Brown L, Sampath R. Localized inferior orbital fibrosis associated with porcine dermal collagen xenograft orbital floor implant. Ophthal Plast Reconstr Surg 20: 257-259. 2004.

Chiquet-Ehrismann R, Hagios C, Matsumoto K. The tenascin gene family. Perspect Dev Neurobiol 2: 3-7. 1994.

Claes L, Burri C, Kiefer H, Mutschler W. Resorbable implants for refixation of osteochondral fragments in joint surfaces. Aktuelle Traumatol 16: 74-77. 1986.

Converse JM, Smith B. Enophthalmos and diplopia in fractures of the orbital floor. Br J Plast Surg 9: 265-274. 1957.

Converse JM, Smith B, Obear MF, Wood-Smith D. Orbital blowout fractures: A ten year survey. Plast Reconstr Surg 39: 20-23. 1967.

Cordewener FW, Bos RR, Rozema FR, Houtman WA. Poly(L-lactide) implants for repair of human orbital floor defects: clinical and magnetic resonance imaging evaluation of long-term results. J Oral Maxillofac Surg 54: 9-13. 1996.

Cordewener FW, Rozema FR, Bos RRM, Grijpma DW, Boering G, Pennings AJ. Material properties and tissue reaction during degradation of poly (96L/4D-lactide), a study in vitro and in rats. J Mat Science Mat Med 6: 211-217. 1995.

Cutright DE, Hunsuck EE: The repair of fractures of the orbital floor using biodegradable polylactic acid. Oral Surg 33: 28-34. 1972.

Dechow PC, Schwartz Dabney CL, Ashman RB. Elastic Properties of the Human Mandibular Corpus. In: Bone dynamics in orthodontic and orthopaedic treatment. Cranio-Facial Growth Series, Vol 27. University of Michigan, Ann Arbor, USA. 1992.

de Koomen HA, Stoelinga PJ, Tideman H, Huybers TJ. Interposed bone-graft augmentation of the atrophic mandible (a progress report). J Maxillofac Surg 7:129-135. 1979.

de Roche R, Adolphs N, Kuhn A, Gogolewski S, Hammer B, Rahn B. Reconstruction of the orbits with polylactate implants: animal experimental results after 12 months and clinical prospects. Mund Kiefer Gesichtschir 5: 49-56. 2001.

de Roche R, Kuhn A, de Roche-Weber P, Gogolewski S, Printzen G, Geissmann A, De Jager M, Hammer B, Prein J, Rahn B. Experimental reconstruction of the sheep orbit with biodegradable implants. Mund Kiefer Gesichtschir 2 Suppl 1: 117-120. 1998.

de Visscher JG, van der Wal KG. Medial orbital wall fracture with enophthalmos. J Craniomaxillofac Surg. 16: 55-59. 1988.

Dempf R, Gockeln R, Schierle HP. Autogene Knochentransplantate zur Versorgung der traumatisch geschädigten orbita. Ophthalmologe 98: 178-184. 2001.

Doddi N, Versfelt CC, Wasserman D. Synthetic absorbable surgical devices of poly-dioxanone. US Pat. no. 4052988. 1977.

Dolores W, Christian R, Harald N, Hildegunde P, Georg W. Cellular and molecular composition of fibrous capsules formed around silicone breast implants with special focus on local immune reactions. J Autoimmun 23: 81-91. 2004.

Dufresne CR, Manson PN, Iliff NT. Early and late complications of orbital fractures. Clin Plast Surg 15: 239-253. 1988.

Egbert M, Stoelinga PJ, Blijdorp PA, de Koomen HA. The "three-piece" osteotomy and interpositional bone graft for augmentation of the atrophic mandible. J Oral Maxillofac Surg 44: 680-687. 1986.

Ehrlich HP. Wound closure evidence of cooperation between fibroblasts and collagen matrix. Eye 2: 149-157. 1988.

Ellis E III, Tan Y. Assessment of internal orbital reconstruction for pure blowout fractures: Cranial bone grafts versus titanium mesh. J Oral Maxillofac Surg 61: 442-453. 2003.

Enislidis G, Pichorner S, Kainberger F, Ewers R. Lactosorb panel and screws for repair of large orbital floor defects. J Craniomaxillofac Surg 25: 316-321. 1997.

Fearon JA, Munro IR, Bruce DA. Observations on the use of rigid fixation for craniofacial deformities in infants and young children. Plast Reconstr Surg. 954: 634-637. 1995.

Fischer EW, Sterzel HJ, Wegner G. Koll. Z. Z. Polym 251: 980-990. 1973.

Frazza EJ, Schmitt EE. A new absorbable suture. J Biomed Mater Res 5: 43-58. 1971.

Friesenecker J, Dammer R, Moritz M, Niederdellmann H. Long-term results after primary restoration of the orbital floor. J Cranio Max-Fac Surg 23: 31-33. 1995.

Fujino T, Makino K. Entrapment mechanism and ocular injury in orbital blowout fracture. Plast Reconstr Surg 65: 571-576. 1980.

Fujino T. Experimental "blowout" fracture of the orbit. Plast Reconstr Surg 54: 81-82. 1974.

Furusawa T, Mizunuma K. Osteoconductive properties and efficacy of resorbable bioactive glass as a bone-grafting material. Implant Dent 6: 93-101. 1997.

Gailit J, Clark RA. Wound repair in the context of extracellular matrix. Curr Opin Cell Biol 6: 717-725. 1994.

Gilbard SM, Mafee MF, Lagouros PA, Langer BG. Orbital blowout fractures. The prognostic significance of computed tomography. Ophthalmology 92: 1523-1528. 1985.

Glassman RD, Manson PN, Vanderkolk CA, Iliff NT, Yaremchuk MJ, Petty P, Defresne CR, Markowitz BL. Rigid fixation of internal orbital fractures. Plast Reconstr Surg 86: 1103-1109. 1990.

Gogolewsky S, Jovanovic M, Perren SM, Dillon JG, Hughes MK. Tissue response and in vivo degradation of selected polyhydroxyacids: polylactides (PLA), poly (3-hydroxybutyrate) (PHB), and poly(3-hydroxybutyrate-co-3-hydroxyvalerate) (PHB/VA). J Biomed Mater Res 27: 1135-1148. 1993.

Goodman SB. The effects of micromotion and particulate materials on tissue differentiation. Bone chamber studies in rabbits. Acta Orthop Scand Suppl 258: 1-43. 1994.

Govender S, Csimma C, Genant HK, Valentin-Opran A, Amit Y, Arbel R, Aro H, Atar D, Bishay M, Borner MG, Chiron P, Choong P, Cinats J, Courtenay B, Feibel R, Geulette B, Gravel C, Haas N, Raschke M, Hammacher E, van der Velde D, Hardy P, Holt M, Josten C, Ketterl RL, Lindeque B, Lob G, Mathevon H, McCoy G, Marsh D, Miller R, Munting E, Oevre S, Nordsletten L, Patel A, Pohl A, Rennie W, Reynders P, Rommens PM, Rondia J, Rossouw WC, Daneel PJ, Ruff S, Ruter A, Santavirta S, Schildhauer TA, Gekle C, Schnettler R, Segal D, Seiler H, Snowdowne RB, Stapert J, Taglang G, Verdonk R, Vogels L, Weckbach A, Wentzensen A, Wisniewski T. Recombinant human bone morphogenetic protein-2 for treatment of open tibial fractures: a prospective, controlled, randomized study of four hundred and fifty patients. J Bone Joint Surg Am. 84: 2123-2134. 2002.

Greenwald HS Jr, Keeney AH, Shannon GM. A review of 128 patients with orbital fractures Am J Ophthalmol 78: 655-664.1974.

Gross U, Strunz V. The interface of various glasses and glass ceramics with a bony implantation bed. J Biomed Mater Res 19: 251-271. 1985.

Gysi A. Studies on the leverage problem of the mandible. Dent Digest 27: 74-84, 144-150, 203-208. 1921.

Haers PE, Sailer HF. Biodegradable self-reinforced poly-L/DL-lactide plates and screws in bimaxillary orthognathic surgery: short term skeletal stability and material related failures. J Craniomaxillofac Surg 26: 363-372. 1998.

Haers PE, Suuronen R, Lindqvist C, Sailer H. Biodegradable polylactide plates and screws in ortognathic surgery: technical note. J Craniomaxillofac Surg 26: 87–91. 1998.

Hammerschlag SB, Hughes S, O'Reilly GV, Naheedy MH, Rumbaugh CL. Blow-out fractures of the orbit: a comparison of computed tomography and conventional radiography with anatomical correlation. Radiology 143: 487-492. 1982.

Hemprich A, Breier T. Secondary correction of traumatic enophthalmos with auto- and alloplastic implants. Rev Stomatol Maxillofac 194: 37-39. 1993.

Hench LL, Paschall HA. Direct chemical bond of bioactive glass-ceramic materials to bone and muscle. J Biomed Mater Res 7: 25-42. 1973.

Hes J, de Man K. Use of blocks of hydroxylapatite for secondary reconstruction of the orbital floor. Int J Oral Maxillofac Surg 19: 275-278. 1990.

Hidding J, Deitmer T, Hemprich A, Ahrberg W. Primary correction of orbital fractures using PDS-foil. Fortschr Kiefer Gesichtschir 36: 195-196. 1991.

Holten CH. Lactic acid. Weinheim: Verlag Chemie 221-231. 1971.

Howeedy AA, Virtanen I, Laitinen L, Gould NS, Koukoulis GK, Gould VE. Differential distribution of tenascin in the normal, hyperplastic, and neoplastic breast. Lab Invest 63: 798-806. 1990.

Huygh A, Schepers EJ, Barbier L, Ducheyne P. Microchemical transformation of bioactive glass particles of narrow size range, a 0-24 months study. J Mater Sci Mater Med 13: 315-320. 2002.

Hylander WL. The human mandible: Lever or link? Am J Phys Anthrop 43: 227-242. 1975.

Hylander WL. In-vivo bone strain in the mandible of Galago crassicaudatus. Am J Phys Anthrop 46: 309-326. 1977.

Iatrou I, Theologie-Lygidakis N, Angelopoulos A. Use of membrane and bone grafts in the reconstruction of orbital fractures. Oral Surg Oral Med Oral Pathol Oral Radiol Endod 91: 281-285. 2001.

Iizuka T, Mikkonen P, Paukku P, Lindqvist C. Reconstruction of orbital floor with polydioxanone plate. Int J Oral Maxillofac Surg 20: 83-87. 1991.

Ilankovan V, Jackson IT. Experience in the use of calvarial bone grafts in orbital reconstruction. Br J Oral Maxillofac Surg 30: 92-94. 1992.

Jank S, Emshoff R, Schuchter B, Strobl H, Brandlmaier I, Norer B. Orbital floor reconstruction with flexible Ethisorb patches: a retrospective long-term follow-up study. Oral Surg Oral Med Oral Pathol Oral Radiol Endod 95:16-22. 2003.

Jin HR, Shin SO, Choo MJ, Choi YS. Relationship between the extent of fracture and the degree of enophthalmos in isolated blowout fractures of the medial orbital wall. J Oral Maxillofac Surg 58: 617-620. 2000.

Jones DE, Evans JN. "Blow-out" fractures of the orbit: an investigation into their anatomical basis. J Laryngol Otol 81: 1109-1120. 1967.

Jordan DR, St Onge P, Anderson RL, Patrinely JR, Nerad JA. Complications associated with alloplastic implants used in orbital fracture repair. Ophthalmology 99: 1600-1608. 1992.

Karesh JW, Horswell BB. Correction of late enophthalmos with polyethylene implant. J Craniomaxillofac Trauma 2: 18-23. 1996.

Katou F, Andoh N, Motegi K, Nagura H. Immuno-inflammatory responses in the tissue adjacent to titanium miniplates used in the treatment of mandibular fractures. J Craniomaxillofac Surg 24: 155-162. 1996.

Kaye BL. Orbital floor repair with antral wall bone grafts. Plast Reconstr Surg 37: 62-65. 1966.

Kinnunen I, Aitasalo K, Pöllönen M, Varpula M. Reconstruction of orbital floor fractures using bioactive glass. J Craniomaxillofac Surg 28: 229-234. 2000.

Knoop M, Lunstedt B, Thiede A. Maxon and PDS--evaluation and physical and biologic properties of monofilament absorbable suture materials. Langenbecks Arch Chir 371:13-28. 1987.

Kobayashi AS, Woo SL, Lawrence C, Schlegel WA. Analysis of the corneo-scleral shell by the method of direct stiffness. J Biomechanics 4: 323-330. 1971.

Konttinen YT, Li TF, Mandelin J, Ainola M, Lassus J, Virtanen I, Santavirta S, Tammi M, Tammi R. Hyaluronan synthases, hyaluronan, and its CD44 receptor in tissue around loosened total hip prostheses. J Pathol 194: 384-390. 2001.

Konttinen YT, Li TF, Michelsson O, Xu JW, Sorsa T, Santavirta S, Imai S, Virtanen I. Expression of tenascin-C in aseptic loosening of total hip replacement. Ann Rheum Dis 57: 619-623. 1998.

Koorneef L, Zonneveld FW. The role of direct multiplanar high resolution CT in the assessment and management of orbital trauma. Radiol Clin North Am. 4: 753-759. 1987.

Korioth TW, Versluis A. Modeling the mechanical behaviour of the jaws and their related structures by finite element (FE) analysis. Crit Rev Oral Biol Med 8: 90-104. 1997.

Kranau R, Klesper B, Hillner D, Reinhardt R. Langzeitergebnisse nach orbitatrummerfrakturen unter besonderer berucksichtigung der orbitabodenrekonstruktion mit einer resorbierbaren PDS-platte. In Schwenzer N, Pfeifer G eds.: Fortschritte der Kiefer- und Gesichts-Chirurgie. Georg Thieme Verlag Stuttgart-New York. 217-218. 1991.

Ksander GA, Vistnes LM. The incidence of experimental contracture varies with the source of the prosthesis. Plast Reconstr Surg 75: 668-676. 1985.

Kulkarni RK, Moore EG, Hegyeli AF, Leonard F. Biodegradable poly(lactic acid) polymers. J Biomed Mater Res 5: 169-181. 1971.

Kupersmith MJ, Fazzone HE. Comparing ocular muscle limitation tests for clinical trial use. Arch Ophthalmol 122: 347-348. 2004.

Lai A, Gliklich RE, Rubin PA. Repair of orbital blow-out fractures with nasoseptal cartilage. Laryngoscope 108: 645-650. 1998.

Lanyon LE. Functional stress in bone tissue as an objective, and a controlling stimulus for adaptive bone remodelling. J Biomech 20: 1083-1093. 1987.

Lee HH, Alcaraz N, Reino A, Lawson W. Reconstruction of orbital floor fractures with maxillary bone. Arch Otolaryngol Head Neck Surg 124: 56-59. 1998.

Lemke BN, Kikkawa DO. Repair of orbital floor fractures with hydroxyapatite block scaffolding. Ophthal Plast Reconstr Surg 15: 161-165. 1999.

Linder L, Lundskog J. Incorporation of stainless steel, titanium and Vitallium in bone. Injury 6: 277-285. 1975.

Lindholm TC, Gao TJ, Lindholm TS. Time-related deviations of fibronectin and type I, II and III collagen on the interface between a hydroxyapatite disc and the rim of a calvarial trephine defect in rabbits. Biomaterials 17: 1515-1520. 1996.

Lossing C, Hansson HA. Peptide growth factors and myofibroblasts in capsules around human breast implants. Plast Reconstr Surg. 91: 1277-1286. 1993.

Luomanen M, Virtanen I. Fibronectins in healing incision, excision and laser wounds. J Oral Pathol Med 20: 133-138. 1991.

Luomanen M, Virtanen I. Distribution of tenascin in healing incision, excision and laser wounds. J Oral Pathol Med 22: 41-45. 1993.

Mackenzie DJ, Arora B, Hansen J. Orbital floor repair with titanium mesh screen. J Craniomaxillofac Trauma 5: 9-16. 1999.

Mackie EJ, Halfter W, Liverani D. Induction of tenascin in healing wounds. J Cell Biol 107: 2757-2767. 1988.

Mäkelä P, Pohjonen T, Törmälä P, Waris T, Ashammakhi N. Strength retention properties of self-reinforced poly L-lactide (SR-PLLA) sutures compared with polyglyconate (Maxon) and polydioxanone (PDS) sutures. An in vitro study. Biomaterials. 23: 2587-2592. 2002.

Mäkelä EA, Vainionpää S, Vihtonen K, Mero M, Helevirta P, Törmälä P, Rokkanen P. The effect of a penetrating biodegradable implant on the growth plate. An experimental study on growing rabbits with special reference to polydioxanone. Clin Orthop 241: 300-308. 1989.

Makita Corp. Makita product catalogue, Aichi, Japan 1996.

Manfre L, Nicoletti G, Lombardo M, Consoli V, Pero G, Albanese V. Orbital “blow-in” fracture: MRI. Neuroradiology 35: 612-613. 1993.

Manson PN, Grivas A, Rosenbaum A, Vannier M, Zinreich J, Iliff N. Studies on enophthalmos: II. The measurement of orbital injuries and their treatment by quantitative computed tomography. Plast Reconstr Surg 77: 203-214. 1986.

Marx RE. Clinical application of bone biology to mandibular and maxillary reconstruction. Clin Plast Surg 21: 377-392. 1994.

Merten HA, Luhr HG. Resorbable synthetics (PDS foils) for bridging extensive orbital wall defects in an animal experiment comparison. Fortschr Kiefer Gesichtschir 39: 186-190. 1994.

Mintz SM, Ettinger A, Schmakel T, Gleason MJ. Contralateral coronoid process bone grafts for orbital floor reconstruction: an anatomic and clinical study. J Oral Maxillofac Surg. 56: 1140-1144. 1998.

Moberg LE, Nordenram Å, Kjellman O: Metal release from plates used in jaw fracture treatment. A pilot study. Int J Oral Surg 18: 311-314. 1989.

Mongini F, Calderale PM, Barberi G. Relationship between structure and the stress pattern in the human mandible. J Dent Res 58: 2334 - 2337. 1979.

Morax S, Hurbli T, Smida R. Bovine heterologous bone graft in orbital surgery. Ann Chir Plast Esthet 38: 445-450. 1993.

Morrison AD, Sanderson RC, Moos KF. The use of silastic as an orbital implant for reconstruction of orbital wall defects: review of 311 cases treated over 20 years. J Oral Maxillofac Surg 53: 412-417. 1995.

Motoki DS, Mulliken JB. The healing of bone and cartilage. Clin Plast Surg. 17: 527-544. 1990.

Nagelschmidt M, Becker D, Bonninghoff N, Engelhardt GH. Effect of fibronectin therapy and fibronectin deficiency on wound healing: a study in rats. J Trauma 27: 1267-1271. 1987.

Ono I, Gunji H, Suda K, Kaneko F, Yago K. Orbital reconstruction with hydroxyapatite ceramic implants. Scand J Plast Reconstr Surg Hand Surg 28: 193-198. 1994.

Onodera K, Ooya K, Kawamura H. Titanium lymph node pigmentation in the reconstruction plate system of a mandibular bone defect. Oral Surg Oral Med Oral Pat 75: 495-497. 1993.

Pauzie F, Cheynet F, Chossegros C, Aldegheri A, Carreau JP, Blanc JL. Long-term complications of silicone implants used in the repair of fractures of the orbital floor. Rev Stomatol Chir Maxillofac. 98: 109-115. 1997.

Peltola M, Suonpaa J, Aitasalo K, Varpula M, Yli-Urpo A, Happonen RP. Obliteration of the frontal sinus cavity with bioactive glass. Head Neck 20: 315-319. 1998.

Pfeiffer RL. Traumatic enophthalmos. Arch Ophth 30: 718-726. 1943.

Pieron AP, Bigelow D, Hamonic M. Bone grafting with Boplant. Results in thirty-three cases. J Bone Joint Surg Br 50: 364-368. 1968.

Pistner H, Bendix DR, Muhling J, Reuther JF. Poly(L-lactide): a long term degradation study in vivo. Biomaterials 14: 671-677. 1993.

Plaga BR, Royster RM, Donigian AM, Wright GB, Caskey PM. Fixation of osteochondral fractures in rabbit knees. A comparison of Kirschner wires, fibrin sealant, and polydioxanone pins. J Bone Joint Surg Br 74: 292-296. 1992.

Pohjonen, T. SR-PLLA:n valmistus, rakenne ja ominaisuudet. LicTech Thesis. Tampere University of Technology 1995.

Power ED. A nonlinear finite element model of the human eye to investigate ocular injuries from night vision goggles. MD thesis, Virginia Polytechnic Institute and State University, USA. 2001.

Putterman AM, Stevens T, Urist MJ. Nonsurgical management of blow-out fractures of the orbital floor. Am J Ophthalmol 77: 232-239. 1974.

Putterman AM. The conservative approach. Management of blow out fractures of the orbital floor. Survey Ophthalmol 35: 292-298. 1991.

Raghow R. The role of extracellular matrix in postinflammatory wound healing and fibrosis. FASEB J 8: 823-831. 1994.

Ralph JP, Caputo AA. Analysis of stress patterns in the human mandible. J Dent Res 54: 814-821. 1975.

Ravosa MJ, Noble VE, Hylander WL, Johnson KR, Kowalski EM. Masticatory stress, orbital orientation and the evolution of the primate postorbital bar. J Hum Evol 38: 667-693. 2000.

Ray JA, Doddi N, Regula D, Williams JA, Melveger A. Polydioxanone (PDS), a novel monofilament synthetic absorbable suture. Surg Gynecol Obstet 153: 497-507. 1981.

Reno F, Lombardi F, Cannas M. UHMWPE oxidation increases granulocytes activation: a role in tissue response after prosthesis implant. Biomaterials 24: 2895-2900. 2003.

Rhee JS, Kilde J, Yoganadan N, Pintar F. Orbital blowout fractures: experimental evidence for the pure hydraulic theory. Arch Facial Plast Surg 4: 98-101. 2002.

Riedl J, Genelin A. Treatment of acromioclavicular dislocations by a pin and tension band fixation. Unfallchirurgie. Jun; 17:140-145. 1991.

Robinson M. The temporomandibular joint: Theory of reflex controlled non-lever action of the mandible. J Am Dent Assoc 33: 1260-1271. 1946.

Romano JJ, Iliff NT, Manson PN. Use of Medpor porous polyethylene implants in 140 patients with facial fractures. J Craniofac Surg 4: 142-147. 1993.

Roncevic R, Malinger B. Experience with various procedures in the treatment of orbital floor fractures. J Maxillofac Surg 9: 81-84. 1981.

Roy DM, Linnehan SK. Hydroxyapatite formed from coral skeletal carbonate by hydrothermal exchange. Nature 247: 220-222. 1974.

Rozema FR, Bos RR, Pennings AJ, Jansen HW. Poly(L-lactide) implants in repair of defects of the orbital floor: an animal study. J Oral Maxillofac Surg 48: 1305-1309. 1990.

Rubin JP, Yaremchuk MJ. Complications and toxicities of implantable biomaterials used in facial reconstructive and aesthetic surgery: a comprehensive review of the literature. Plast Reconstr Surg 100: 1336-1353. 1997.

Rubin PA, Bilyk JR, Shore JW. Orbital reconstruction using porous polyethylene sheets. Ophthalmology 101: 1697-1708. 1994.

Rubin PA. Shore JW, Yaremchuck MJ. Complex orbital fracture repair using rigid fixation of the internal orbital skeleton. Ophthalmology 99: 553-557. 1992.

Santavirta S, Lappalainen R, Pekko P, Anttila A, Konttinen YT. The counterface, surface smoothness, tolerances, and coatings in total joint prostheses. Clin Orthop 369: 92-102. 1999.

Santavirta S, Xu JW, Hietanen J, Ceponis A, Sorsa T, Kontio R, Konttinen YT. Activation of periprosthetic connective tissue in aseptic loosening of total hip replacements. Clin Orthop 352: 16-24. 1998.

Sargent LA, Fulks KD. Reconstruction of internal orbital fractures with Vitallium mesh. Plast Reconstr Surg 88: 31-38. 1991.

Sasserath C, Van Reck J, Gitani J. The use of a polyglycolic acid membrane in the reconstruction of the orbital floor and in loss of bone substance in the maxillofacial region. Acta Stomatol Belg 88: 5-11. 1991.

Sauerland EK. Grant's dissector. Williams & Wilkins, Baltimore, USA. 1994.

Schepers EJ, Ducheyne P, Barbier L, Schepers S. Bioactive glass particles of narrow size range: a new material for the repair of bone defects. Implant Dent 2: 151-156. 1993.

Shannon C, Thull R, von Recum A. Types I and III collagen in the tissue capsules of titanium and stainless-steel implants. J Biomed Mater Res 4: 401-408. 1997.

Siddique SA, Mathog RH. A comparison of parietal and iliac crest bone grafts for orbital reconstruction. J Oral Maxillofacial Surg 60: 44-50. 2002.

Smith B, Regan WF. Blow-out fracture of the orbit. Am J Ophth 6: 733-739. 1957.

St John TA, Vaccaro AR, Sah AP, Schaefer M, Berta SC, Albert T, Hilibrand A. Physical and monetary costs associated with autogenous bone graft harvesting. Am J Orthop 32: 18-23. 2003.

Standlee JP, Caputo AA, Ralph JP. The condyle as a stress-distributing component of the temporomandibular joint. J Oral Rehab 8: 391-400. 1981.

Sugar AW, Kuriakose M, Walshaw ND. Titanium mesh in orbital wall reconstruction. Int J Oral Maxillofac Surg 21: 140-144. 1992.

Sullivan PK, Rosenstein DA, Holmes RE, Craig D, Manson PN. Bone-graft reconstruction of the monkey orbital floor with iliac grafts and titanium mesh plates: a histometric study. Plast Reconstr Surg 91: 769-775. 1993.

Suuronen R. Biodegradable fracture fixation devices in maxillofacial surgery. Int J Oral Maxillofac Surg 22: 50–57. 1993.

Suuronen R, Pohjonen T, Hietanen J, Lindqvist C. A 5-year in vitro and in vivo study of the biodegradation of polylactide plates. J Oral Maxillofac Surg 56: 604-614. 1998.

Tadjoedin ES, de Lange GL, Holzmann PJ, Kulper L, Burger EH. Histological observations on biopsies harvested following sinus floor elevation using a bioactive glass material of narrow size range. Clin Oral Implants Res 11: 334-344. 2000.

Tams J, Rozema FR, Bos RR, Roodenburg JL, Nikkels PG, Vermey A. Poly(L-lactide) bone plates and screws for internal fixation of mandibular swing osteotomies. Int J Oral Maxillofac Surg 25: 20-24. 1996.

Taylor SR, Gibbons DF. Effect of surface texture on the soft tissue response to polymer implants. J Biomed Mater Res 17: 205-227. 1983.

Tessier P. Complications of facial trauma: principles of late reconstruction. Ann Plast Surg 17: 411-420. 1986.

Thadani V, Penar PL, Partington J, Kalb R, Janssen R, Schonberger LB, Rabkin CS, Prichard JW. (36c) Creutzfeldt-Jakob disease probably acquired from a cadaver dura mater graft. Case report. J Neurosurg 69: 766-669. 1988.

Thaller SR, Moore C, Tesluk H. Biodegradable polyglyconate plates and screws: a histological evaluation in a rabbit model. J Craniofac Surg 6: 282-287. 1995.

Tideman H, Samman N, Cheung LK. Functional reconstruction of the mandible: a modified titanium mesh system. Int J Oral Maxillofac Surg 27: 339-345. 1998.

Tiitta O, Wahlstrom T, Paavonen J, Linnala A, Sharma S, Gould VE, Virtanen I. Enhanced tenascin expression in cervical and vulvar koilocytotic lesions. Am J Pathol 141: 907-913. 1992.

Tong L, Bauer RJ, Buchman SR. A current 10-year retrospective survey of 199 surgically treated orbital floor fractures in a nonurban tertiary care center. Plast Reconstr Surg 108: 612-621. 2001.

Törmälä P, Pohjonen T, Rokkanen P. Bioabsorbable polymers: materials technology and surgical applications. Proceedings of the Institution of Mechanical Engineering. Part H-J Eng Med 212: 101-111. 1998.

Uchio E, Onho S, Kudoh K, Andoh K, Kisielewicz LT. Simulation of Air bag impact on a post-radial keratectomy by finite element analysis method. J Cataract Refrac Surg 28: 1847-1853. 2001.

Uchio E, Watanabe Y, Kadonosono K, Matsuoka Y, Goto S. Simulation of air bag impact on eyes after photorefractive keratectomy by finite element analysis method. Arch Clin Exp Ophthalmol 241: 497-504. 2003.

Urist MR. Bone: Formation by autoinduction. 1965. Clin Orthop 395: 4-10. 2002.

Vainionpää S, Rokkanen P, Törmälä P. Surgical applications of biodegradable polymers in human tissues. Progr Polym Sci 14: 679-716. 1989.

van Mullem PJ, Vaandrager JM, Nicolai JP, de Wijn JR. Implantation of porous acrylic cement in soft tissues: an animal and human biopsy histological study. Biomaterials 11: 299-304. 1990.

Vartio T, Laitinen L, Närvänen O, Cutola M, Thornell LE, Zardi L, Virtanen I. Differential expression of the ED sequence-containing form of cellular fibronectin in embryo and human tissue. J Cell Sci 88: 419-422. 1987.

Vert M, Chabot F, Leray J, Christel P. 116a Stereoregular bioresorbable polyesters for orthopaedic surgery. Macromol Chem Phys Suppl 5: 30-41. 1981.

Ward WK, Slobodzian EP, Tiekotter KL, Wood MD. The effect of microgeometry, implant thickness and polyurethane chemistry on the foreign body response to subcutaneous implants. Biomaterials 23: 4185-4192. 2002.

Waterhouse N, Lyne J, Urdang M, Garey L. An investigation into the mechanism of orbital blowout fractures. Br J Plast Surg 52: 607-612. 1999.

Webster K. Orbital floor repair with lyophilized porcine dermis. Oral Surg Oral Med Oral Pathol 65: 161-164. 1988.

Welch MP, Odland GF, Clark RA. Temporal relationships of F-actin bundle formation, collagen and fibronectin matrix assembly, and fibronectin receptor expression to wound contraction. J Cell Biol 110: 133-145. 1990.

Whitby DJ, Ferguson MW. The extracellular matrix of lip wounds in fetal, neonatal and adult mice. Development 112: 651-668. 1991.

Williams DF. Review. Biodegradation of surgical polymers. J Materials Science 17: 1233-1246. 1982.

Wilson J, Pigott GH, Schoen FJ, Hench LL. Toxicology and biocompatibility of bioglasses. J Biomed Mater Res 15: 805-817. 1981.

Wiltfang J, Merten HA, Becker HJ, Luhr HG. The resorbable miniplate system Lactosorb in a growing cranio-osteoplasty animal model. J Craniomaxillofac Surg 27: 207-210. 1999.

Ylikontiola L, Sundqvist K, Sandor GK, Törmälä P, Ashammakhi N. Self-reinforced bioresorbable poly-L/DL-lactide [SR-P(L/DL)LA] 70/30 miniplates and miniscrews are reliable for fixation of anterior mandibular fractures: a pilot study. Oral Surg Oral Med Oral Pathol Oral Radiol Endod 97:312-7. 2004.

Zhan Y, Engel M, Kujat C, Backens M, Kubale R, Kramann B. Proton spin tomography of the orbit in post-traumatic motility disorders. Rofo Fortschr Geb Röntgenstr Neuen Bildgeb Verfahr 163: 127-133. 1995.